JOURNAL OF GEOPHYSICAL RESEARCH, VOL. 113, A06218, doi:10.1029/2007JA012768, 2008

Parametric analysis of positive amplitude electron acoustic solitary waves in a magnetized plasma and its application to boundary layers

S. S. Ghosh,[1] J. S. Pickett,[2] G. S. Lakhina,[1] J. D. Winningham,[3] B. Lavraud,[4] and P. M. E. Décréau[5]

Received 27 August 2007; revised 5 November 2007; accepted 19 December 2007; published 20 June 2008.

[1] The existence domain of a fully nonlinear positive amplitude electron acoustic solitary wave has been studied in a four-component plasma composed of warm magnetized electrons, warm electron beam, and energetic multi-ion species with ions hotter than the electrons ($T_i > T_e$). A Sagdeev pseudopotential technique has been used to obtain the nonlinear evolution equation for the wave propagating obliquely with the ambient magnetic field. It is observed that the ion temperatures and concentrations play a crucial role in determining the characteristics and the existence domain of the electron acoustic solitary wave. With a large cold ion population and/or a large cold to hot ion temperature ratio, the plasma tends to behave like a single ion-dominated one. The corresponding Sagdeev pseudopotential shows an extremely narrow and deep profile producing small-amplitude, narrow width, spiky solitary waves. Such solutions are found to be applicable in the bow shock, magnetosheath, and cusp regions. Comparison with CLUSTER observations agrees well with the analytical model. It has been shown that in the magnetosheath, cooler He^{2+} ions are necessary to produce a positive polarity solution while a hotter species may produce a compressive (negative polarity) solution.

Citation: Ghosh, S. S., J. S. Pickett, G. S. Lakhina, J. D. Winningham, B. Lavraud, and P. M. E. Décréau (2008), Parametric analysis of positive amplitude electron acoustic solitary waves in a magnetized plasma and its application to boundary layers, *J. Geophys. Res.*, *113*, A06218, doi:10.1029/2007JA012768.

1. Introduction

[2] Solitary waves have been identified throughout the Earth's magnetosphere at narrow boundaries and in strong currents. Plasma wave measurements of the GEOTAIL spacecraft [*Matsumoto et al.*, 1994b] revealed broadband electrostatic noise (BEN) emissions as a series of electrostatic solitary waves (ESWs) [*Matsumoto et al.*, 1994a]. The associated electric field intensities of the BEN range from a few μV/m to 100 mV/m [*El-Taibany*, 2005]. High time resolution data analysis indicated small-scale, large-amplitude electric fields in the auroral acceleration region [*Temerin et al.*, 1982; *Böstrom et al.*, 1988; *Mozer et al.*, 1997; *Ergun et al.*, 1998a; *Bounds et al.*, 1999; *Pottelette et al.*, 1999; *McFadden et al.*, 1999], in the plasma sheet boundary layer (PSBL) [*Matsumoto et al.*, 1994a], in the Earth's high-altitude polar magnetosphere [*Franz et al.*, 1998], in the polar cap boundary layer (PCBL) [*Tsurutani et al.*, 1998], in the bow shock [*Matsumoto et al.*, 1997; *Bale et al.*, 1998], and on cusp field lines [*Pickett et al.*, 1999; *Cattell et al.*, 1999, 2001]. They have also been seen in Saturn's magnetosphere [*Williams et al.*, 2006] and in the solar wind and heliosphere [*Mangeney et al.*, 1999; *Williams et al.*, 2005]. Recent observations of the CLUSTER satellites show the presence of numerous electrostatic solitary waves with very short time duration in the magnetosheath [*Pickett et al.*, 2003, 2004]. Nonlinear processes, such as beam instabilities or acoustic instabilities, have been proposed as the generation mechanism of such spiky structures. Whereas a two stream instability gives rise to a BGK mode phase space hole, an acoustic instability may lead to either ion or electron mode solitary waves representing density enhancements and depletions. Solitary waves have also been observed to be associated with reconnection at the dayside and in the magnetotail [*Deng et al.*, 2004; *Cattell et al.*, 2005]. It is mostly recognized that the observed fast moving positive polarity pulses are governed by the electron dynamics. *Dubouloz et al.* [1991b] interpreted them as electron acoustic solitons, whereas *Muschietti et al.* [1999] modeled them as localized nonlinear BGK phase space electron holes [*Dupree*, 1982]. Discovery of solitary waves in BEN emission triggered a series of simulation works by *Matsumoto et al.* [1994a], *Omura et al.* [1994], and several other researchers in order to explore their generation mechanisms [*Goldman et al.*, 1999; *Muschietti et al.*, 1999; *Singh*, 2000; *Newman et al.*, 2001]. In most cases, their works have been focused on the generation of phase space holes. The presence of highly energetic ions in the different regions of the magnetosphere, however,

[1] Indian Institute of Geomagnetism, Navi Mumbai, India.
[2] University of Iowa, Iowa City, Iowa, USA.
[3] Southwest Research Institute, San Antonio, Texas, USA.
[4] Los Alamos National Laboratory, Los Alamos, New Mexico, USA.
[5] LPCE et Université d'Orléans, Orléans, France.

0148-0227/08/2007JA012768$09.00

motivated us to study the electron acoustic wave in further detail.

[3] An electron acoustic mode was first identified by *Fried and Gould* [1961] during numerical solutions of the linear electrostatic Vlasov dispersion equation in a homogeneous unmagnetized plasma. It is a high-frequency acoustic-like wave which is governed by the electron dynamics. *Gary and Tokar* [1985] showed that it is a weakly damped mode in a two electron temperature plasma where cold electrons provide the restoring force and the pressure is provided by the hot electrons. A linear electron acoustic wave may also be excited in the presence of energetic ions where typically ions have greater thermal energy than electrons ($T_i > T_e$) [*Lashmore-Davies and Martin*, 1973]. This also gives credence to the existence of the electron acoustic mode in the PCBL [*Tsurutani et al.*, 1998] and magnetotail [*Baumjohann et al.*, 1989] where ions are observed to be more energetic than electrons. Both linear [*Watanabe and Taniuti*, 1977; *Yu and Shukla*, 1983; *Tokar and Gary*, 1984; *Gary and Tokar*, 1985; *Mace and Hellberg*, 1990; *Singh and Lakhina*, 2001] and nonlinear [*Buti et al.*, 1980; *Buti*, 1980; *Mace et al.*, 1991; *Dubouloz et al.*, 1991b, 1993; *Mace and Hellberg*, 1993; *Berthomier et al.*, 2000; *Singh et al.*, 2001; *Mamun and Shukla*, 2002a, 2002b] theories of electron acoustic waves have been developed by many authors. This theory has also been successfully applied to interpret different magnetospheric phenomena [*Tokar and Gary*, 1984; *Lin et al.*, 1985; *Schriver and Ashour-Abdalla*, 1987; *Bharuthram and Shukla*, 1988; *Dubouloz et al.*, 1991a, 1991b; *Pottelette et al.*, 1999; *Singh and Lakhina*, 2001; *Singh et al.*, 2001]. The relatively high frequency of the ESWs and the presence of counterstreaming electrons [*Parks et al.*, 1984; *Schriver and Ashour-Abdalla*, 1987] further support the existence of electron acoustic solitons in the PSBL. One weak point of such a model was the absence of positive amplitude solitary waves in previous theoretical analysis [*Dubouloz et al.*, 1991b; *Mace et al.*, 1991; *Singh and Lakhina*, 2004]. In our previous work, we have overcome this discrepancy by assuming a simple analytical model which supports the existence of positive amplitude electron acoustic solitary waves [*Ghosh and Lakhina*, 2005a, 2005b]. The model describes obliquely propagating solitary waves in a magnetized plasma consisting of energetic ions. It also indicates that a positive amplitude wave is a more favorable solution compared to a negative one which is consistent with the observations. The corresponding width-amplitude characteristics are found to agree well with the FAST observations [*Ghosh and Lakhina*, 2005b; *Ergun et al.*, 1998b]. In the present work, we have further studied the parametric variations and existence domain of such positive polarity solutions. It is observed that the presence of the multi-ion species plays a crucial role in determining both the characteristics of the solitary wave and its existence domain. As the plasma approaches to a single-ion population, extremely narrow and spiky structures are obtained indicating a special type of solitary solution. Unlike the usual bell-shaped profiles, they show cusp-like structures and are essentially of small amplitudes. Such solutions are relevant for the recent observations of the bow shock and magnetosheath regions where the plasma is composed of protons with a small percentage of hot He^{2+} ions.

[4] The paper is organized as follows. In the next section (section 2), the fully nonlinear Sagdeev pseudopotential has been derived analytically for a four component plasma and the conditions for the critical Mach number have been obtained analytically. In section 3, parametric effects on the electron acoustic solitary wave solution have been studied extensively for both multi-ion (section 3.1) and single ion (section 3.3) plasmas including double layers (section 3.2). In section 4 we have compared our analytical results with recent spacecraft observations while an overall discussion has been presented in section 5.

2. Derivation of the Sagdeev Pseudopotential

[5] In the present analysis, fully nonlinear solutions for electron acoustic solitary waves have been obtained for a magnetized plasma using the Sagdeev pseudopotential technique [*Ghosh and Lakhina*, 2004]. The magnetic field is parallel to the z direction and the wave is propagating obliquely in the y-z plane with an angle θ with the ambient magnetic field. The wave is governed by electron dynamics. The plasma is assumed to be infinite, one-dimensional, and collisionless. It consists of hot, energetic, multi-ion species, and warm electrons and traversed by a warm electron beam parallel to the magnetic field. The electrons are assumed to be adiabatic ($\gamma = 3$) and the ions are hotter than the electrons ($T_i > T_e$). We have assumed that the plasma consists of two ion species, namely, a heavier ion species, which can either be oxygen (O) or helium (He) ions, and hydrogen (H) ions. Both the heavier and the lighter ion species are separately in thermal equilibrium obeying the Boltzmann distribution and the heavier ions (e.g., oxygen ions for the present case) are cooler than hydrogen. The governing fluid equations are

$$\frac{\partial N_{eb}}{\partial t} + \frac{\partial}{\partial z}(N_{eb} v_{ebz}) = 0, \tag{1}$$

$$\frac{\partial v_{ebz}}{\partial t} + v_{ebz}\frac{\partial v_{ebz}}{\partial z} = \frac{\partial \phi}{\partial z} - 3\sigma_{eb} N_{eb}\frac{\partial N_{eb}}{\partial z}, \tag{2}$$

$$\frac{\partial N_{es}}{\partial t} + \nabla \cdot (N_{es} v_{\mathbf{es}}) = 0, \tag{3}$$

$$\frac{\partial v_{\mathbf{es}}}{\partial t} + (v_{\mathbf{es}} \cdot \nabla) v_{es} = \nabla\phi - 3\sigma_{es} N_{es} \nabla N_{es} - \alpha_e (v_{\mathbf{es}} \times b), \tag{4}$$

with the ion density of

$$\begin{aligned} n_i &= n_{iO} + n_{iH} \\ &= z_1 \mu_i e \exp\left[-z_1\left(\frac{\phi}{z_1^2\mu_i + z_2^2\nu_i\beta_i}\right)\right] \\ &\quad + z_2 \nu_i e \exp\left[-z_2\left(\frac{\beta_i\phi}{z_1^2\mu_i + z_2^2\nu_i\beta_i}\right)\right] \end{aligned} \tag{5}$$

where the subscripts *i*, *e*, *eb* (*es*), *ic* (*ih*) denote ion, electron, beam (bulk) electrons, and cooler (hotter) ions, respectively,

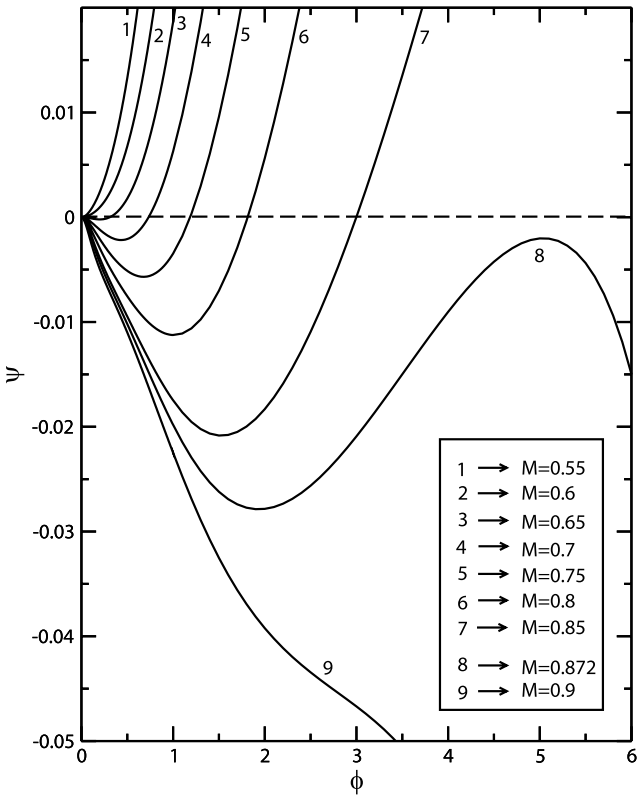

Figure 1. Sagdeev pseudopotentials for positive amplitude electron acoustic solitary waves for different Mach numbers. The multi-ion plasma consists of oxygen and hydrogen ions ($z_1 = 1$, $z_2 = 1$) with $\mu_i = 0.2$ and $\beta_i = 1/40$. The beam (bulk) electron temperatures are σ_{eb} (σ_{es}) = 1/40 (1/20), respectively, and bulk electron concentration $\rho_{es} = 0.75$. The wave is propagating with an obliqueness of $\theta = 60°$ and the speed of electron beam is $u_{eb} = 0.5$. The parameter $\alpha_e = 0.5$.

the subscript z denotes the z component of the velocity, $N_{ej} = n_{ej}/\rho_{ej}$ ($j = b, s$) and z_1 (z_2) are the charge multiplicities of cooler (hotter) ions. The parameters ρ_{eb} (ρ_{es}) are the ambient densities of beam (bulk) electrons, $\sigma_{eb,es}$(= $T_{eb,es}/T_{iff}$) are the beam, bulk electron to ion temperature ratios, $T_{iff}\left(=\frac{T_{ic}T_{ih}}{z_1^2\mu_i T_{ih}+z_2^2\nu_i T_{ic}}\right)$ is the effective ion temperature, μ_i (ν_i) are the ambient densities of the cooler (hotter) ion species, namely the oxygen (hydrogen) ions, β_i(=T_{ic}/T_{ih}) is the cooler to hotter ion temperature ratio (i.e., oxygen to hydrogen temperature ratio for the present case), u_{eb} is the initial velocity of the beam electrons, and α_e(=Ω_{ce}/ω_{pe}) denotes the ratio of the electron cyclotron and electron plasma frequencies. The beam electrons are assumed to have only the z component of motion which is justified considering their highly magnetized state and very small Larmour radius [*Sutradhar and Bujarbarua*, 1988]. All the number densities are normalized to the equilibrium plasma density n_0 ($z_1\mu_i + z_2\nu_i = \rho_{eb} + \rho_{es} = 1$), the electron pressure p_{ej} ($j = b, s$) is normalized to electron equilibrium pressure p_0(=n_0T_e, $T_e = \rho_{eb}T_{eb}+\rho_{es}T_{es}$) and other variables, namely, t, x, $v_{eb,es}$, and ϕ are normalized to the reciprocal of electron plasma frequency ω_{pe}^{-1} ($\omega_{pe} = \sqrt{\frac{4\pi n_0 e^2}{m_e}}$), effective ion Debye length λ_{Diff}(=$\sqrt{\frac{T_{iff}}{4\pi n_0 e^2}}$), effective electron acoustic speed c_{iff}(=$\sqrt{\frac{T_{iff}}{m_e}}$) and $\frac{T_{iff}}{e}$, respectively. The Mach number M is also normalized by c_{iff} and $\boldsymbol{b} = (0, 0, 1)$ is normalized by the ambient magnetic field B_0. As in the case of ion acoustic waves [*Ghosh and Lakhina*, 2004], we assume the quasi-neutrality condition [*Buti*, 1980] which implies that

$$n_i = z_1 n_{ic} + z_2 n_{ih} = n_{eb} + n_{es}. \tag{6}$$

[6] We assume the following normalized boundary conditions:

$$\begin{aligned} &at\ |x| \to \infty\ ,\ v_{eb} \to u_{eb}\ ,\ v_{es} \to 0 \\ &\sum_{j=b,s} p_{ej} \to 1\ ,\ N_{ej} \to 1 \quad and \quad \phi \to 0, \end{aligned} \tag{7}$$

which also implies that

$$at\ \ |x| \to \infty\ ,\ p_{ej} \to \rho_{ej}\frac{T_{ej}}{T_e}\ , \quad and\ \ n_{ej} \to \rho_{ej}. \tag{8}$$

The stationary state solution is obtained by assuming the transformation

$$\eta = k_y y + k_z z - Mt, \tag{9}$$

where M is the Mach number for the electron acoustic wave and $k_{y,z}$ are the corresponding direction cosines for the oblique propagation.

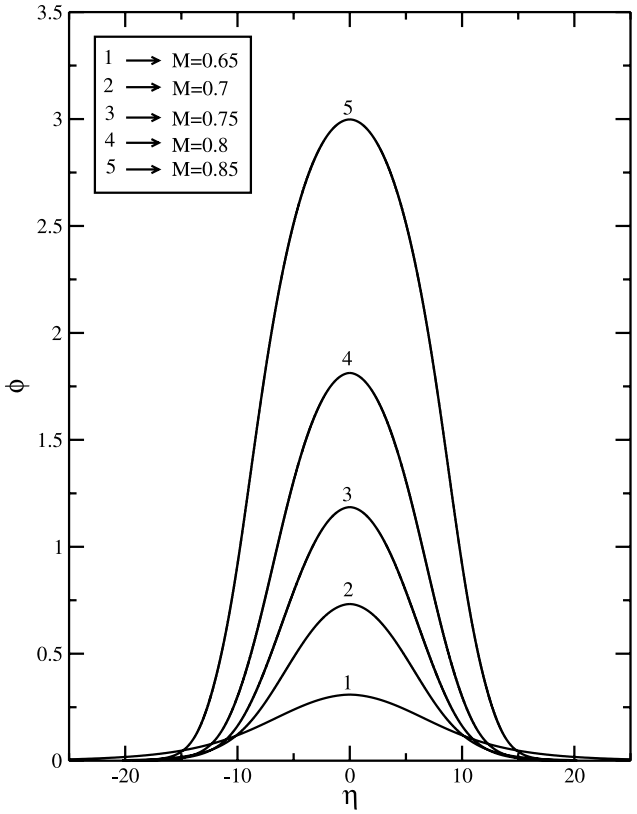

Figure 2. Potential profiles for positive amplitude electron acoustic solitary waves for different Mach numbers. The parameter domain is the same as Figure 1.

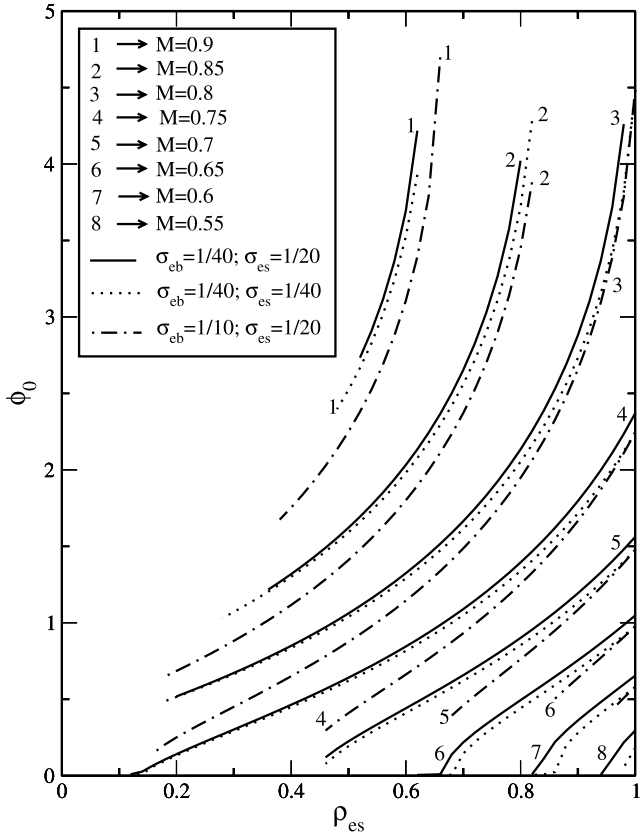

Figure 3. Variation of the amplitude (ϕ_0) with bulk electron concentration (ρ_{es}) for different M. The solid (σ_{eb} = 1/40, σ_{es} = 1/20), dot-dashed (σ_{eb} = 1/10, σ_{es} = 1/20), and dotted (σ_{eb} = 1/40, σ_{es} = 1/40) curves represent different combinations of beam and bulk electron temperatures. Other parameters are the same as Figure 1.

[7] Using equation (9), equations (1)–(4) reduce to

$$\frac{d}{d\eta}\left[\frac{1}{2}\frac{1}{N_{es}}\frac{d^2}{d\eta^2}\left\{\left(\frac{M}{N_{es}}\right)^2+3\sigma_{es}N_{es}^2-2\phi\right\} +\alpha_e^2\left\{\frac{1}{N_{es}}+\frac{k_z^2}{M^2}\left(\sigma_{es}N_{es}^3-N'_{es}\right)\right\}\right]=0, \tag{10}$$

where

$$N'_{es}=\int N_{es}d\phi.$$

Solving the coupled equations (6) and (10), we get

$$\frac{1}{2}\left(\frac{d\phi}{d\eta}\right)^2+\psi(\phi)=0, \tag{11}$$

where $\psi(\phi)$ is the corresponding Sagdeev pseudopotential for an electron acoustic wave,

$$\psi(\phi)=V_e(\phi)\frac{L_e(\phi)}{H_e(\phi)}, \tag{12}$$

$V_e(\phi)$, $L_e(\phi)$, $H_e(\phi)$ being functions of ϕ, M and other parameters.

$$\begin{aligned} V_e(\phi)&=\alpha_e^2N_{es}^6,\\ H_e(\phi)&=\left[\left(3\sigma_{es}N_{es}^4-M^2\right)\frac{dN_{es}}{d\phi}-N_{es}^3\right]^2,\\ L_e(\phi)&=\left[-k_y^2\phi+\frac{1}{2}M^2\left(\frac{s_e}{N_{es}}\right)^2+3h_e+w_e\right]\\ &\quad+k_z^2\left[-h_e+\frac{1}{N_{es}}\left(\sigma_{es}s_e-s'_e\right)+\frac{1}{2}\left(\frac{w_e}{M}\right)^2\right] \end{aligned} \tag{13}$$

where

$$\begin{aligned} &s_e=N_{es}-1\,,\quad s'_e=N'_{es}-\delta\,,\quad \delta=N'_{es}|_{\phi=0}\,,\\ &h_e=\frac{1}{2}\sigma_{es}\left(N_{es}^2-1\right),\quad w_e=s'_e-\sigma_{es}\left(N_{es}^3-1\right);\\ &N_{eb}=\frac{1}{2\sqrt{3\sigma_{eb}}}\left[M_{eb+}\left(1+\frac{2\phi}{M_{eb+}^2}\right)^{1/2}-M_{eb-}\left(1+\frac{2\phi}{M_{eb-}^2}\right)^{1/2}\right];\\ &M_{eb\pm}=\left(\frac{M-k_zu_{eb}}{k_z}\right)\pm\sqrt{3\sigma_{eb}}. \end{aligned}$$

[8] To ascertain the existence of the solitary electron acoustic wave, the Sagdeev pseudopotential [$\psi(\phi)$] should

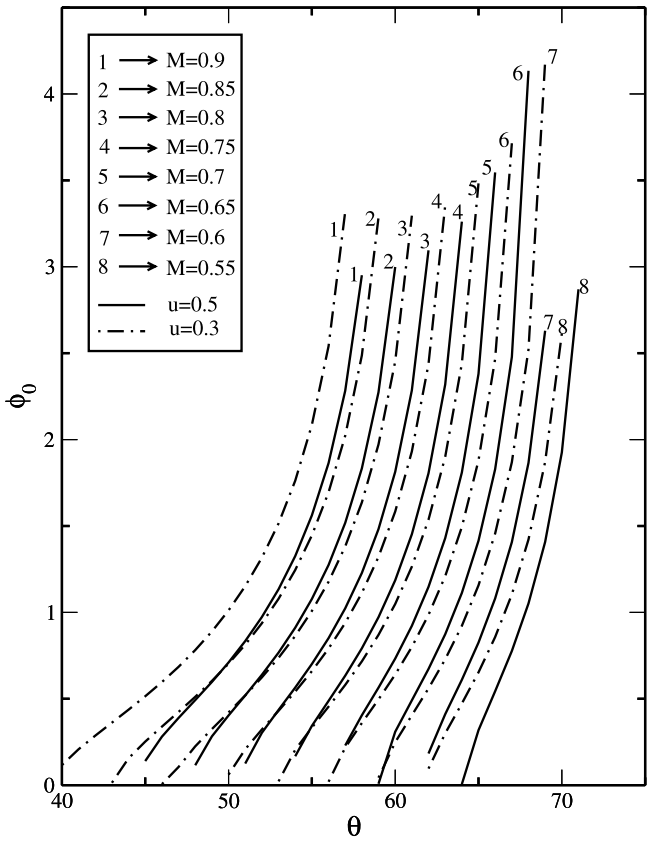

Figure 4. Variation of the amplitude (ϕ_0) with obliqueness (θ) for different M. The solid (u_{eb} = 0.5) and dot-dashed (u_{eb} = 0.3) curves represent two different beam electron velocities, other parameters being the same as Figure 1.

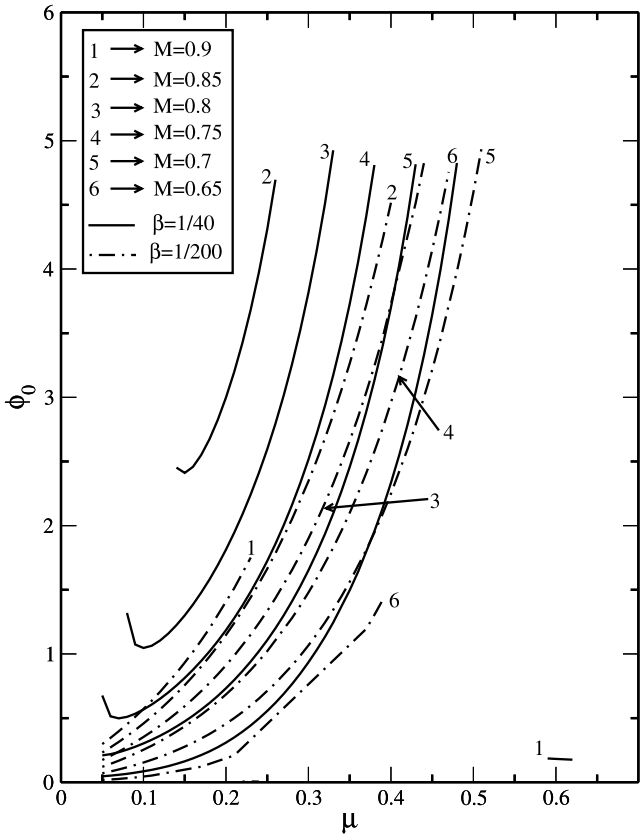

Figure 5. Variation of the amplitude (ϕ_0) with oxygen ion concentration (μ_i) for different M. The solid (β_i = 1/40) and dot-dashed (β_i = 1/200) curves represent two different ion temperature ratios. Other parameters are the same as Figure 1.

satisfy the following boundary conditions [*Ghosh and Iyengar*, 1997]:

$$\psi(\phi)\big|_{\phi=0} = 0\,; \quad \left.\frac{\partial\psi(\phi)}{\partial\phi}\right|_{\phi=0} = 0\,; \quad \left.\frac{\partial^2\psi(\phi)}{\partial\phi^2}\right|_{\phi=0} < 0\,;$$
$$\psi(\phi_0) = 0\,; \quad \psi(\phi) < 0 \ \textit{for}\ \ 0 < |\phi| < |\phi_0| \tag{14}$$

where ϕ_0 is the amplitude of the electron acoustic solitary wave. Putting the conditions in equation (14) into equation (12), we obtain the following inequalities for different parameter regions:

[9] Case a

$$\textit{if}\ \ \frac{\rho_{eb}}{M_{eb}^2 - 3\sigma_{eb}} + \frac{\rho_{es}}{M^2 - 3\sigma_{es}} > 1\,, \quad M > \sqrt{3\sigma_{es}}\,; \quad \textit{or}$$
$$\frac{\rho_{eb}}{M_{eb}^2 - 3\sigma_{eb}} + \frac{\rho_{es}}{M^2 - 3\sigma_{es}} < 1\,, \quad M < \sqrt{3\sigma_{es}}\ ;\ \textit{then}$$
$$\frac{\rho_{eb}}{M_{eb}^2 - 3\sigma_{eb}}\left(1 - 3\sigma_{eb}\frac{k_z^2}{M^2}\right) + \frac{k_z^2}{M^2}(\rho_{es} + 3\sigma_{es}) < 1. \tag{15}$$

Case b

$$\textit{if}\ \ \frac{\rho_{eb}}{M_{eb}^2 - 3\sigma_{eb}} + \frac{\rho_{es}}{M^2 - 3\sigma_{es}} < 1\,, \quad M > \sqrt{3\sigma_{es}}\,; \quad \textit{or}$$
$$\frac{\rho_{eb}}{M_{eb}^2 - 3\sigma_{eb}} + \frac{\rho_{es}}{M^2 - 3\sigma_{es}} > 1\,, \quad M < \sqrt{3\sigma_{es}}\ \ \textit{then}$$
$$\frac{\rho_{eb}}{M_{eb}^2 - 3\sigma_{eb}}\left(1 - 3\sigma_{eb}\frac{k_z^2}{M^2}\right) + \frac{k_z^2}{M^2}(\rho_{es} + 3\sigma_{es}) > 1. \tag{16}$$

The inequality conditions thus obtained determine the existence domain of the corresponding solitary wave solution.

3. Electron Acoustic Solitary Waves

[10] The arbitrary-amplitude solutions for electron acoustic solitary waves have been obtained by plotting the Sagdeev pseudopotential $\psi(\phi)$ as a function of the potential ϕ. The solitary wave solutions are obtained when the condition equation (14) is satisfied. This implies the reflection of the pseudoparticle in the pseudopotential field

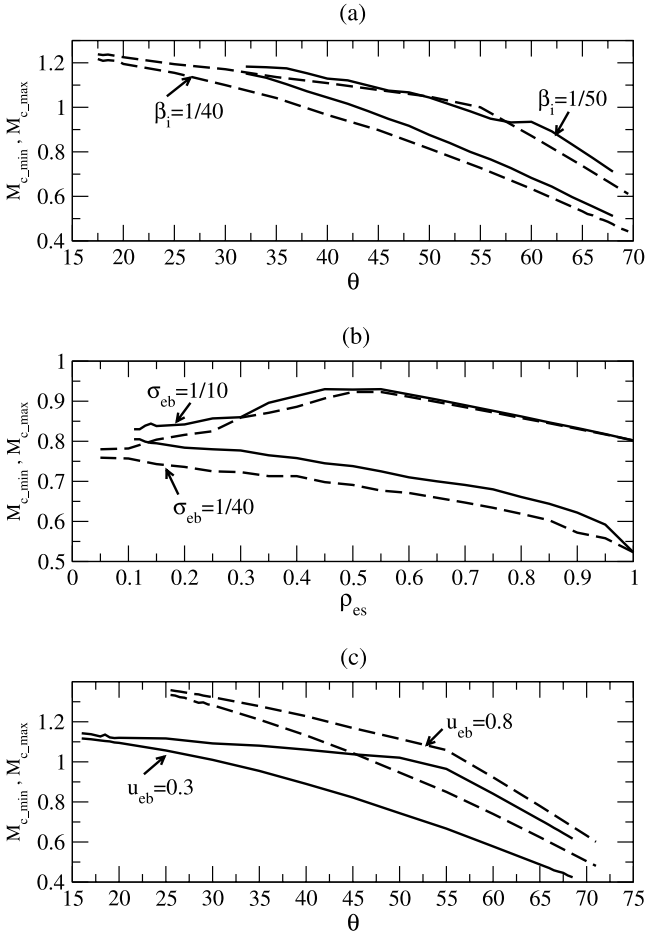

Figure 6. Parametric variations of the existence domains of the positive polarity solutions with (a) θ and β_i; (b) ρ_{es} and σ_{eb}; and (c) θ and u_{eb} in a multi-ion plasma. $M_{c_{min}}$ ($M_{c_{max}}$) denote the minimum (maximum) values of the critical Mach number. All other parameters remain the same as Figure 1.

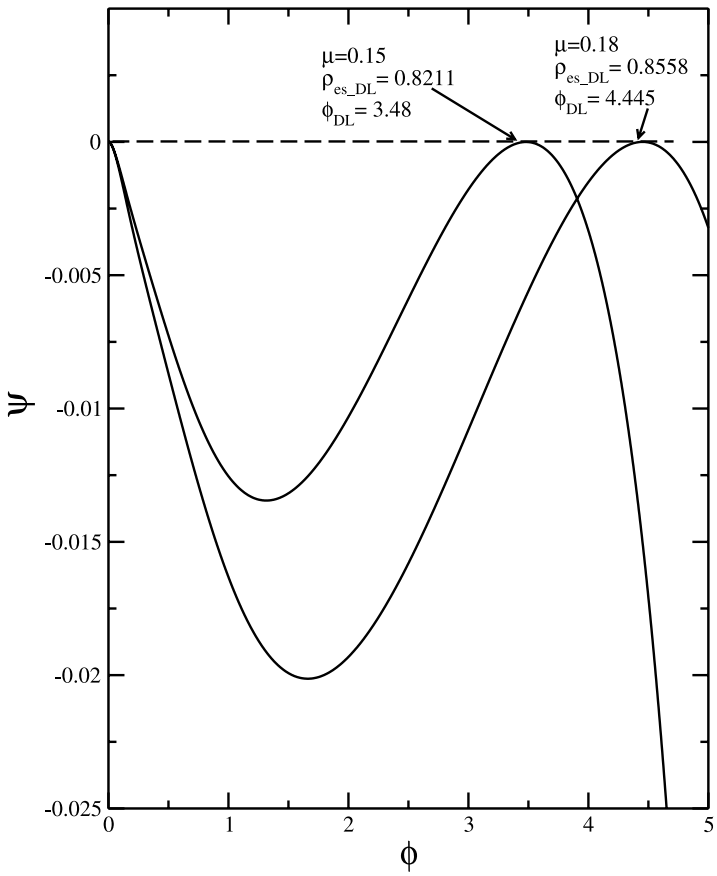

Figure 7. Sagdeev pseudopotentials for double layer solutions for two different μ_i (=0.15 and 0.18, respectively) and $M = 0.84$. Other parameters remain the same as Figure 1.

ensuring the recurrence of the initial state (zero potential drop) for the solitary wave solution. A different class of solutions may also exist for an upper limit of $M = M_{DL}$ where

$$\left.\frac{\partial\psi(\phi)}{\partial\phi}\right|_{\phi=\phi_{DL},M=M_{DL}} = 0\,; \quad \phi_{DL} \neq 0 \tag{17}$$

Under this condition, the imaginary particle is not reflected at $\phi = \phi_{DL}$ because of its vanishing pseudoforce and pseudovelocities. Instead, it goes to another state producing an asymmetrical weak double layer (WDL) with a net potential drop of ϕ_{DL} where ϕ_{DL} is the amplitude of the double layer.

3.1. Multi-Ion Plasma

[11] For the major part of the magnetosphere, the plasma consists of multi-ion species with a minority population of O^+ ions in the cusp or He^{+2} ions in the bow shock and magnetosheath. The presence of such minority components may play a crucial role in determining the plasma properties and the wave generation processes [*Kalra and Kumar*, 2006]. In our present study, we have assumed a multi-ion plasma consisting of hydrogen and oxygen ions with single charge multiplicities (z_1, $z_2 = 1$) while $\alpha_e = 0.5$. Figure 1 shows the Sagdeev pseudopotential curves for electron acoustic solitary waves and Figure 2 shows the corresponding potential profiles obtained numerically by integrating equation (11) with equation (12). Large-amplitude positive polarity solutions are obtained for the varying Mach number. This indicates an overall depletion of the electron density within the perturbed region resulting in a rarefactive solitary wave. Conversely, an overall enhancement of the electron density would result in a negative polarity (compressive wave) solution. For an appropriately large Mach number, the rarefactive electron acoustic solitary wave transforms to an electron acoustic double layer beyond which the solution ceases to exist.

[12] Figure 3 shows the effect of beam and bulk electron temperatures and concentrations on the solitary wave solution. It shows that an increase in the bulk electron concentration increases the potential amplitude. The solid, dot-dashed, and dotted curves represent different combinations of bulk and beam electron temperatures. It is observed that an increase in the beam electron temperature reduces the amplitude (the solid and the dot-dashed curves) while an increase in the bulk electron temperature results in a marginal increase (the solid and the dotted curves). For a large M, solutions terminate for large ρ_{es} as they transform to double layers while for a small M, sufficiently large ρ_{es} is required to initiate the perturbation. This also shows that the effect of beam electrons is significant for the solution. A hotter beam or larger beam electron concentration dampens the wave while, for a fast moving solution, it is necessary to have an adequate

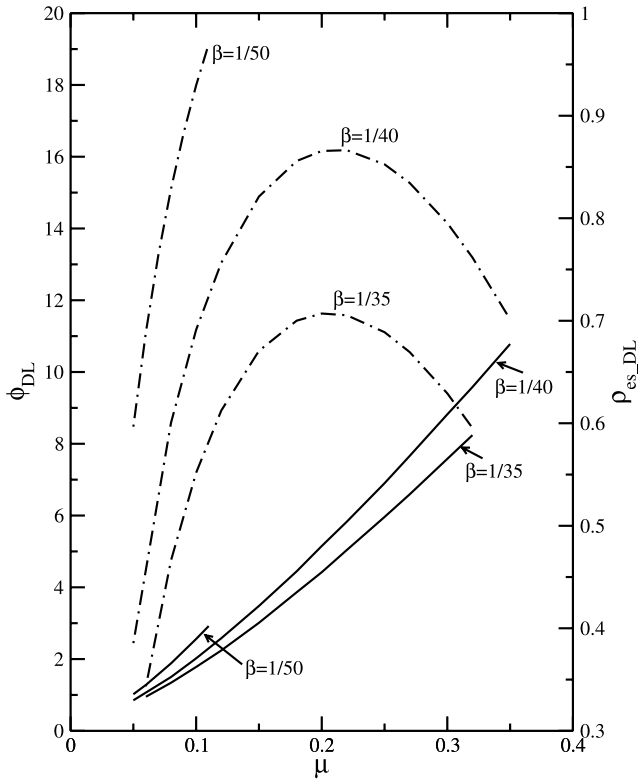

Figure 8. Variation of double layer amplitudes with μ_i for three different β_i. Solid curves show the variation of the amplitude while the dot-dashed curves represent the corresponding bulk electron densities (ρ_{es_DL}) for the double layer. With $M = 0.84$, other parameters remain the same as Figure 1.

electron beam. This also indicates that a fast moving solution is likely to be related to the beam electrons while for a slow moving wave, the effect may not be that significant.

[13] Figure 4 shows the variation of amplitude (ϕ_0) with obliqueness (θ) for two different beam electron speeds (u_{eb}). It shows a sharp increase in the amplitude with increasing obliqueness (θ). The faster solutions (e.g., $M \geq 0.8$) move with lesser obliqueness ($\theta < 60°$) while a slower wave (e.g., $M < 0.8$) moves more obliquely ($\theta > 60°$). The variation becomes much sharper for $\theta > 55°$ while for a smaller angle it shows a moderate variation only. It is further observed that an increase in the beam electron speed (u_{eb}) decreases the amplitude but increases the obliqueness. The solutions are obtained for $35° < \theta < 75°$ which remains consistent with the recent CLUSTER observations [*Pickett et al.*, 2008] (see also sections 4.2 and 4.3). For a further increase in θ, and the amplitude, the solution transforms to a double layer.

[14] Figure 5 shows the variation of amplitude with the oxygen (cooler) ion concentration (μ_i). It is observed that an increase in μ_i and β_i increases the amplitude quite significantly. However, large-amplitude solutions do not transform to double layers for varying β_i or μ_i. Instead they exhibit regions of singularities. As the denominator of equation (12) approaches zero, the Sagdeev pseudopotential blows up which terminates the solution. An interesting outcome occurs with a further increase of μ_i, which reveals a reappearance of very small amplitude solitary wave solutions. Such a plasma with large μ_i behaves like a single ion dominated plasma and will be discussed in section 3.3.

[15] Effects of different parameters on the positive polarity solutions are further summarized in Figures 6a–6c where the existence domain for the corresponding solution has been explored for different parameter regions. The limiting (critical) values of Mach numbers M_c are determined from the condition equation (15) where $M > \sqrt{3\sigma_{es}}$ is satisfied. Figures 6a–6c show the variations of $M_{c_{min}}$ ($M_{c_{max}}$), namely, the minimum (maximum) values of M, with different parameters. It clearly shows the gradual increase in the existence domain with increasing obliqueness (θ) (Figures 6a and 6c) and bulk electron concentrations (ρ_{es}) (Figure 6b). While a minimum obliqueness ($\theta > 20°$) is necessary for the generation of the solitary waves, an increase in the obliqueness slows the wave propagation. On the other hand, the presence of a tenuous electron beam enhances the existence domain but its increase in the concentration inhibits

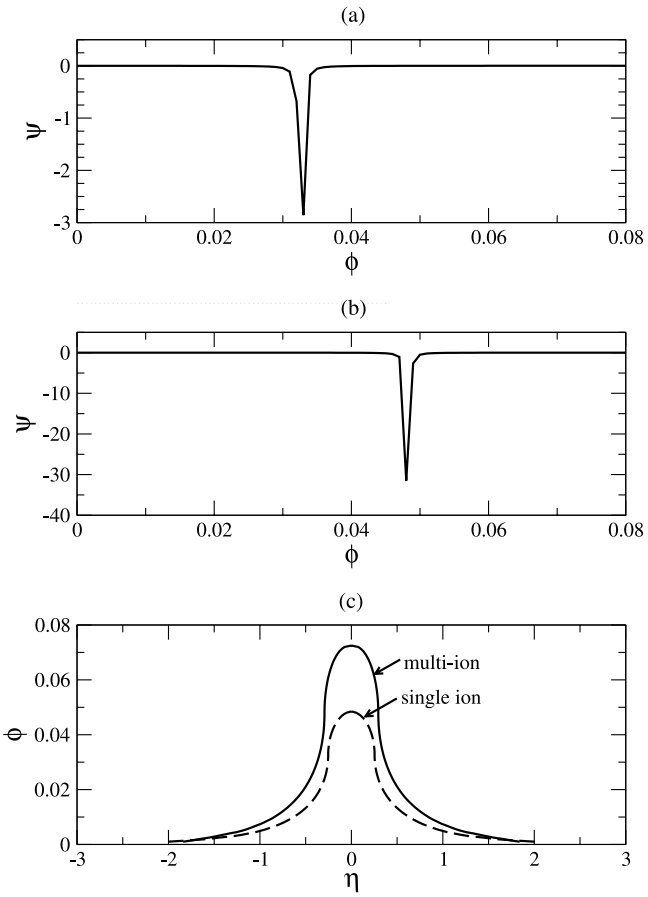

Figure 9. Sagdeev pseudopotential curves for (a) single ion; (b) multi-ion plasmas with exceptionally deep pseudopotential well. (c) The corresponding potential profiles showing cusp-like solitary waves. The solid (dashed) lines correspond to the multi- (single) ion plasmas. The Mach number $M = 0.9$ and the bulk electron concentration $\rho_{es} = 0.55$ for both the cases while for the multi-ion plasma, the cold ion concentration $\mu_i = 0.5$. Other parameters remain the same as Figure 1.

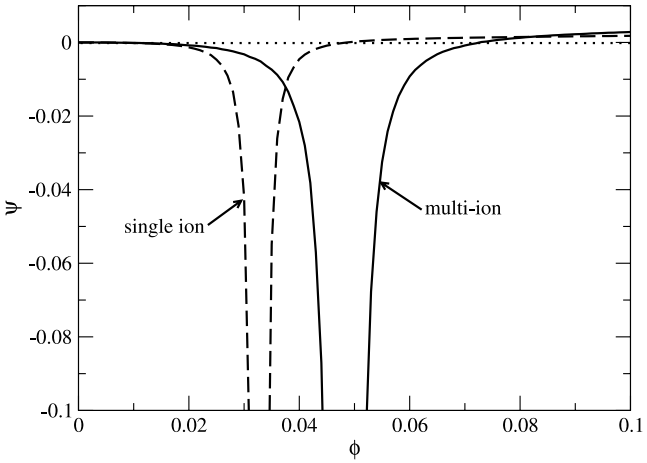

Figure 10. The Sagdeev pseudopotentials of Figures 9a and 9b near the vicinity of $\phi = 0$. The solid (dashed) curves represent the multi- (single) ion plasmas.

the wave formation (Figure 6b). One striking feature is its strong dependence on the ion temperature ratio. While a small decrease in β_i implies the presence of more energetic hydrogen (hotter) ions, it also shrinks the existence domain considerably (Figure 6a). A significant contribution is also observed for the beam electron velocity. While an increase in u_{eb} produces faster waves, it also diminishes the existence domain. Comparatively, an increase in the beam electron temperature moderately increases the lower cut-off value of the critical Mach number ($M_{c_{min}}$) resulting in a decrease in the existence domain while the effect of bulk electron temperatures remains only marginal (Figure 6b).

3.2. Double Layers

[16] As indicated in Figure 1, the rarefactive (positive amplitude) electron acoustic solitary waves transform to double layers for large amplitude solutions. Figure 7 shows the Sagdeev pseudopotential curves for double layer solutions for two different μ_i values. The double layer has been obtained by changing the bulk electron density, M being 0.84. Figure 8 shows the variation of the double

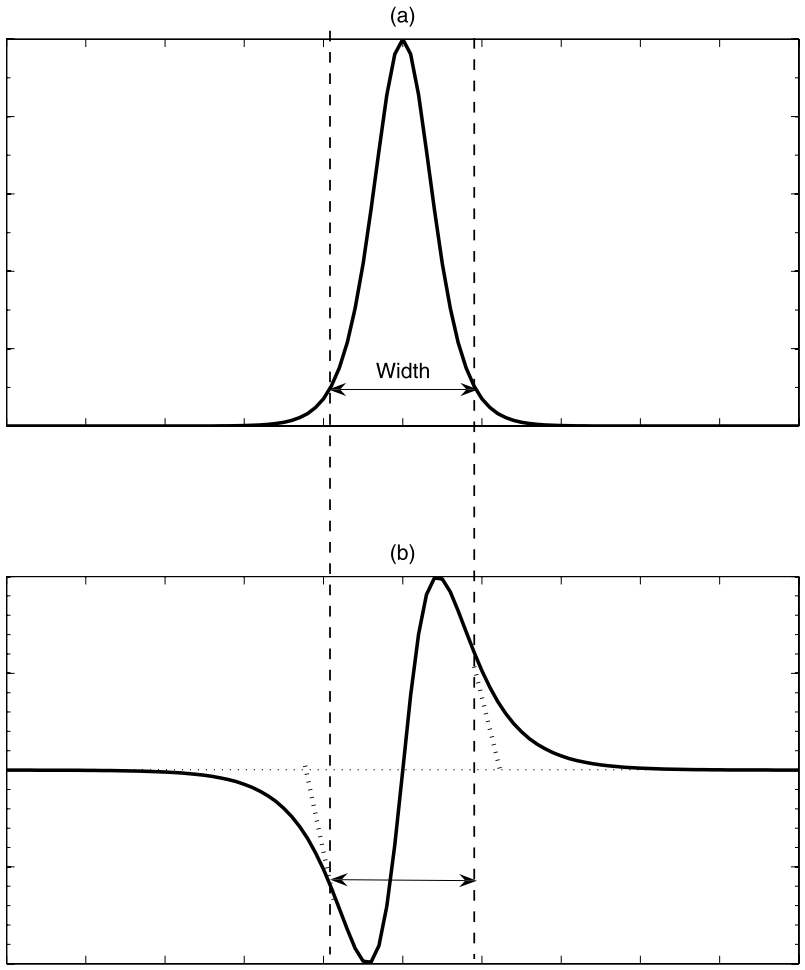

Figure 11. Schematic diagram of (a) the width of the potential profile and (b) the pulse duration of the corresponding electric field. The double arrows show the width (Figure 11a) and the pulse duration (Figure 11b), respectively. The dotted lines in Figure 11b indicate the shape of the observed bipolar pulses.

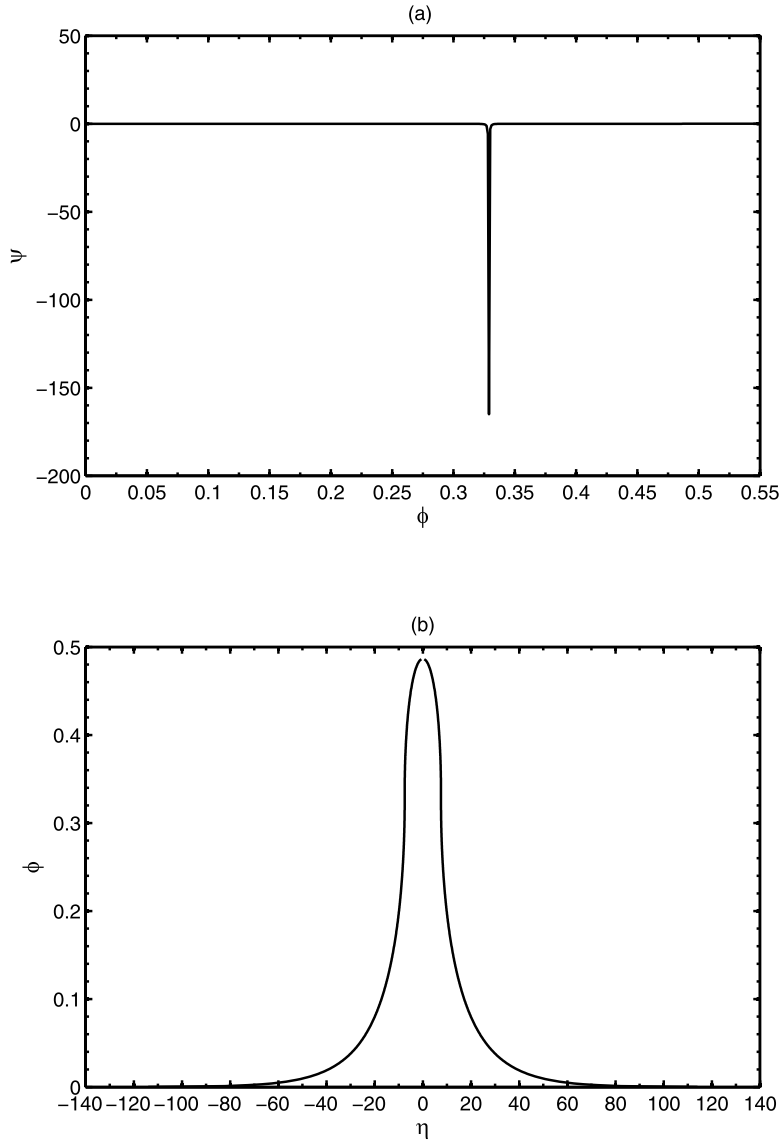

Figure 12. (a) The Sagdeev pseudopotential and (b) the potential profile of the electron acoustic solitary wave in the bow shock transition region. The plasma parameters are $\alpha_e = 0.05$, $\beta_i = 1/4$, $\rho_{es} = 0.98$, $\mu_i = 0.85$, $\sigma_{es} = 0.1079$, $\sigma_{eb} = 0.0863$, $M = 0.77$, $\theta = 75^\circ$, and $u_{eb} = 0.0861$.

layer amplitude with μ_i for three different β_i, namely, $\beta_i = 1/35$, 1/40, and 1/50. Solid curves show the variation of the double layer amplitude while the dot-dashed curve represents the corresponding bulk electron concentration (ρ_{es_DL}). It clearly shows that for a particular M, the double layer solutions are bounded within a very narrow range of β_i ($1/50 \leq \beta_I \leq 1/35$), beyond which no double layer solution exists any more. The amplitude is found to increase with increasing μ_i while the corresponding bulk electron concentration (ρ_{es_DL}) initially increases with μ_i but decreases for large μ_i (>0.2). Interestingly, for $\beta_i = 1/50$, ρ_{es_DL} is almost of the order of 1 and with further increase in μ_i the solution breaks. However, with a larger M (=0.86), it is possible to get a double layer solution with larger μ_i.

3.3. Single Ion Plasma

[17] For a single ion plasma, equation (5) reduces to

$$n_i = \exp(-\phi). \tag{18}$$

The electron acoustic solitary wave solution has been obtained from the corresponding Sagdeev pseudopotential. It has been observed that for a single ion plasma, the variation pattern becomes discontinuous producing regions of ''singularities'' where the Sagdeev pseudopotential blows up owing to its vanishing denominator. In the vicinity of such regions, the pseudopotential has an exceptionally sharp profile which, when integrated, gives an extremely narrow

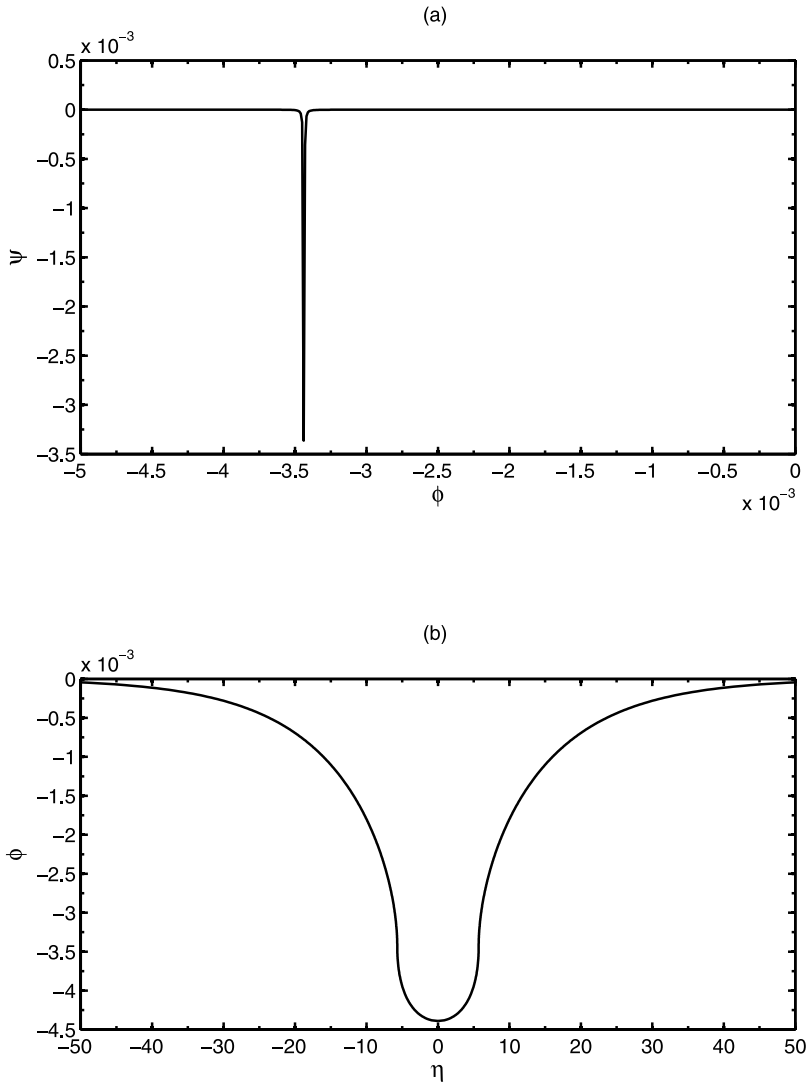

Figure 13. (a) The Sagdeev pseudopotential and (b) the potential profile of the compressive (negative polarity) electron acoustic solitary wave in the magnetosheath. The plasma parameters are $\alpha_e = 0.025$, $\beta_i = 0.54$, $\rho_{es} = 0.65$, $\mu_i = 0.88$, $\sigma_{es} = 0.1969$, $\sigma_{eb} = 0.3988$, $M = 0.9$, $\theta = 30^\circ$ and $u_{eb} = 0.0473$; $T_{He^{+2}} > T_{H^+}$.

cusp-like solution. Such solutions are of small amplitudes and their shapes differ from the usual bell-shaped solitary wave profiles. The cusp-like solitary waves may also exist for a multi-ion plasma for a sufficiently large μ_i. The solution reappears after the breaking of usual large-amplitude solitary wave solutions for increasing μ_i (Figure 5). Figures 9a–9b show the Sagdeev pseudopotential profiles of single and multi-ion plasmas respectively while Figure 9c shows the corresponding potential profiles. The sudden sharp dip in the Sagdeev pseudopotential profile is worthy of being noted. A closer investigation reveals a smooth profile near the vicinity of $\phi = 0$ (Figure 10) which satisfies the conditions of equation (14). *Wei and Chen* [2005], who have studied nonlinear lower hybrid waves in a two ion species plasma, have also indicated the existence of cusp-like solitary waves for "infinite-depth" pseudopotentials. They have pointed out that all the physical quantities within the pseudopotential well remain continuous, thus enabling a physical solution. According to our study, a cusp-like solitary wave is the characteristic of a magnetized plasma and has not been observed for an unmagnetized case. A single ion plasma solely exhibits cusp-like solitary waves while a multi-ion plasma leads to such solutions when it is governed by the large population of cooler components (namely, β_i, $\mu_i \rightarrow 1$). On the other hand, the presence of a small population of cooler component ions is essential to support usual bell-shaped solitary wave profiles. This indicates that the presence of a second ion species plays a key role in determining the characteristics of the solitary wave profile which is further supported by the strong influence of β_i and μ_i on the existence domain. This may also explain the reappearance of the solitary wave with cusp-like profile for a multi-ion plasma with large μ_i since then the plasma tends to be a single ion minimizing the effect of its hotter species.

4. Comparison With Space Observations

[18] Recently, a number of spacecraft missions, such as WIND, GEOTAIL, FAST, POLAR, and CLUSTER, have

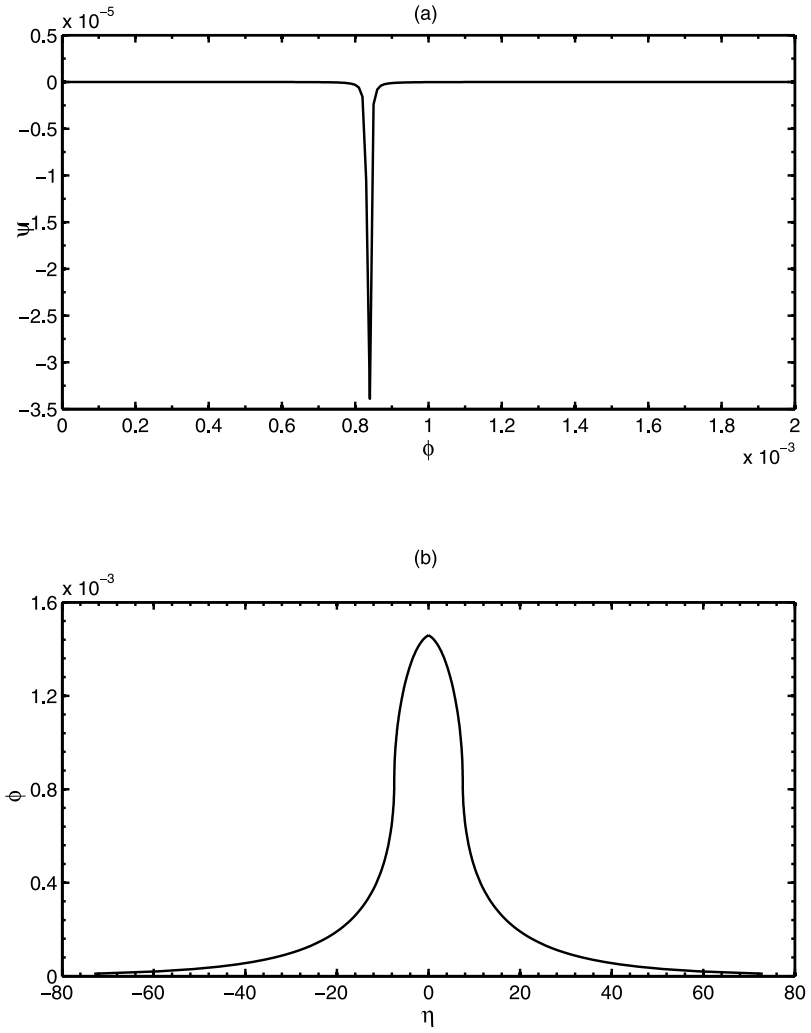

Figure 14. (a) The Sagdeev pseudopotential and (b) the potential profile of the rarefactive (positive polarity) electron acoustic solitary wave in the magnetosheath. The plasma parameters are $\alpha_e = 0.025$, $\beta_i = 0.6$, $\rho_{es} = 0.65$, $\mu_i = 0.1$, $\sigma_{es} = 0.2860$, $\sigma_{eb} = 0.5793$, $M = 0.7$, $\theta = 60°$ and $u_{eb} = 0.0570$; $T_{He^{+2}} < T_{H^+}$.

revealed bipolar and tripolar electrostatic structures with varying field intensities and pulse durations. Positive polarity, high-frequency ESWs have been revealed in the Earth's magnetotail by GEOTAIL [*Matsumoto et al.*, 1994a], in the polar magnetosphere by POLAR [*Franz et al.*, 1998; *Cattell et al.*, 1999], in the midaltitude auroral zone by FAST [*Ergun et al.*, 1998a] and in different regions of the magnetosphere by the CLUSTER multispacecraft mission [*Pickett et al.*, 2003, 2004]. In the latter study, however, the Wideband (WBD) plasma wave receiver obtains electric field measurements along only one axis, that being the average potential between the two electric field spheres and is unable to determine the polarity of the solitary waves. As the plasma conditions vary widely over these regions, the major plasma parameters, such as ambient plasma densities, magnetic fields, and temperatures change significantly inducing changes in the solitary wave potential profile. Studies of such parametrical effects may offer interesting clues to observations. In this section, we have used our aforementioned analytical model to estimate the shape and size of the electron acoustic solitary wave solutions for different regions of space. The nonnormalized values of the width and amplitude have been obtained using the particle data available from observations. We note, however, that the time resolution of the particle measurements is much lower (order of seconds) than that of the WBD measurements of the ESWs (order of microseconds) so that at any instant in time when ESWs are observed, we can only provide the average background particle environment which encompasses a much larger period of time. In the absence of a direct measurement of any specific particle concentration or temperature, it has been estimated from other known parameters assuming some realistic values of β_i, σ_{es}, σ_{eb}, or ρ_{es}. In most cases, the values of M and θ have been presented for a best fitted result. The pulse duration of any solitary structure has been obtained as $\Delta t = |\Delta\eta/M|$, $\Delta\eta$ being the width of the solitary wave, while the average electric field has been obtained as $E = \phi_0/\Delta\eta$. Empirically, we have chosen $\Delta\eta$ as the width of the solitary potential profile at $\phi_w = \phi_0/10$. This choice enabled us to estimate the full width of the corresponding solitary wave profile across the ranges of amplitudes retaining the consistency of the comparisons. Figure 11 shows a schematic

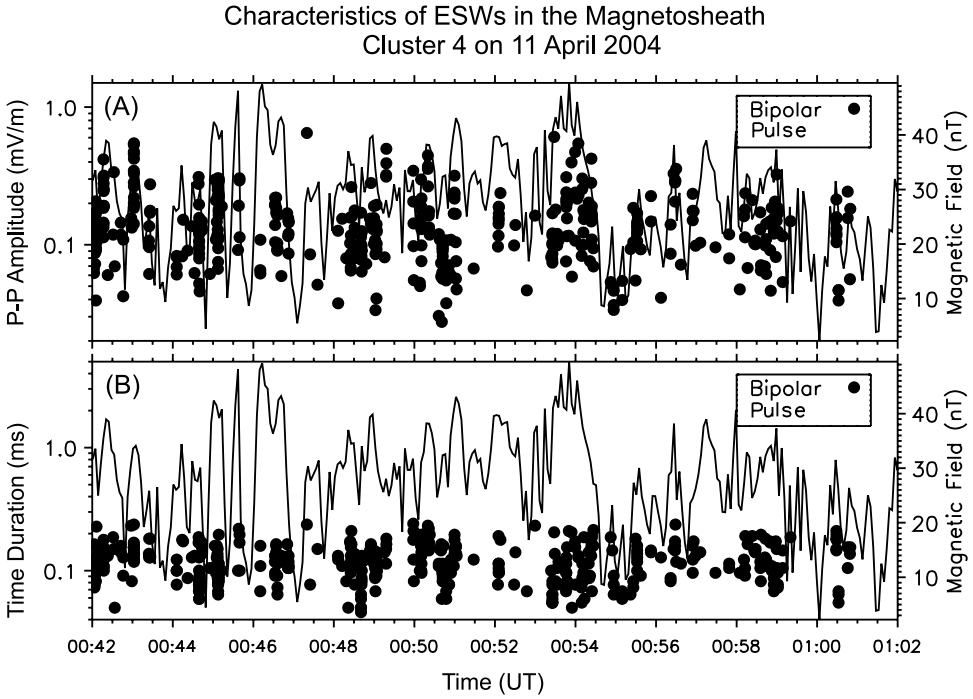

Figure 15. Characteristics of solitary waves at magnetosheath crossing. Black dots represent detections of ESWs of the bipolar type versus time on the horizontal axis. The top panel shows the measured electric field of each ESW with scale on the left vertical axis, and the bottom panel shows the ESW pulse duration with scale on the left vertical axis. The solid line shows the measured magnetic field with its scale on the right vertical axis for each panel (from *Pickett et al.* [2008]).

diagram of the estimated width at $\phi_0/10$ for a sech^2 potential profile and its relation with the pulse duration of the corresponding electric field. Since the measured electric field shows a sharper profile (e.g., dotted lines in Figure 11b), the empirical choice is assumed to be a good approximation for the present case.

4.1. Bow Shock

[19] Intense bipolar structures have been observed in the transition region of the bow shock by the WIND spacecraft [*Bale et al.*, 1998]. Upstream the magnetic field is low and the ions appear with a comparatively narrow energy band. Downstream the magnetic field gets compressed and increased strongly. At the shock transition, the ions get heated producing hotter components at the downstream. The solar wind density also increases and the ion energy spreads over a wider range. The plasma population consists of mainly protons (H^+) with a minority component of He^{+2} ions. The observed ESW shows a wide frequency range. Previous studies have indicated the presence of electron phase space holes [*Bale et al.*, 1998] or electron acoustic waves [*Shin et al.*, 2006] in this region. *Bale et al.* [1998] have reported large-amplitude bipolar field ($E \approx 100$ mV/m) with short pulse duration ($\Delta t \approx 0.1$ ms). The reported electron temperature is of the order of 20–40 eV. We have assumed the bulk (beam) electron temperatures as 35 (28) eV with density ratio 4.9 ($\rho_{es} = 0.98$) and $\tilde{u}_{eb}$ (nonnormalized electron beam velocity) has been taken to be 650 km/s [*Shin et al.*, 2006]. Following *Kalra and Kumar* [2006], we have assumed the existence of the suprathermal particles where ion temperatures lie within 100 eV to 10 keV. We have assumed $T_{He^{+2}} > T_{H^+}$ and $\beta_i = 1/4$, the proton temperature being 300 eV. The ion density ratio is considered to be 11.3 with μ_i for H^+ being 0.85. The ambient plasma density has been estimated from the reported electron Debye length ($\lambda_e = 6.8$ m) [*Bale et al.*, 1998] which is of the order of 40 cm^{-3} and the ambient magnetic field is assumed to be 102 nT, giving rise to $\alpha_e = 0.05$. A positive polarity electron acoustic solitary wave has been obtained for $M = 0.77$ and $\theta = 75°$. Figures 12a and 12b show the respective Sagdeev pseudopotential and potential profile. A very narrow Sagdeev pseudopotential has been obtained with a maximum depth of more than 150 (Figure 12a). The normalized amplitude $\phi_0 = 0.4866$ and width $w = 53.09$ (Figure 12b) which lead to the estimated electric field of $E = 141.06$ mV/m and the pulse duration of $\Delta t = 0.1924$ ms, respectively. The reported ESWs, on the other hand, have shown a maximum amplitude of $E_y = 150$ mV/m and a time duration of $\Delta t \approx 0.1$ ms [*Bale et al.*, 1998] which is quite close to our analytical estimations.

[20] Since an electron acoustic solitary wave is driven by the ion pressure, a large-amplitude indicates a comparatively large ion temperature. Also, the reported electron Debye length has indicated considerably high ambient plasma density. Accordingly, we have chosen a large ambient magnetic field. In such a dense and compressed plasma, high-intensity electric field fluctuation may occur giving rise to large-amplitude electrostatic solitary wave. However, for a more regular case in the solar wind with plasma density of the order of 10–20 cm^{-3} and magnetic field within 10–15 nT, the amplitude is expected to remain of

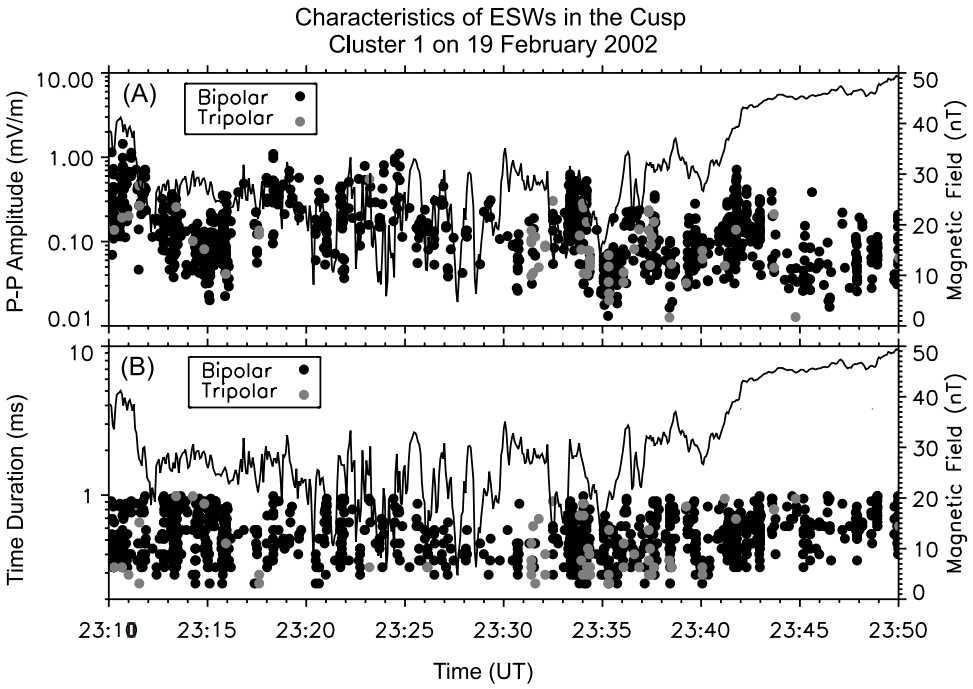

Figure 16. Characteristics of solitary waves at the cusp crossing. Here, gray dots represent detection of tripolar ESWs (see the explanation of the plot in Figure 15 caption).

the order of a few mV/m with a pulse duration of the order of 1 ms.

4.2. Magnetosheath

[21] The WBD plasma wave receiver on the CLUSTER spacecraft [*Gurnett et al.*, 1997] has detected extremely narrow bipolar pulses in the dayside of the magnetosheath. The ESW pulse durations remain the shortest to be measured, being of the order of $\sim$25–100 μs, while the amplitude is typically <1 mV/m [*Pickett et al.*, 2003, 2008]. Such small-amplitude, narrow width pulses are particularly challenging since the usual theory of small-amplitude solitary waves (weakly nonlinear theory) predicts a much wider shape indicating an increase in the solitary width. We have previously shown that a large-amplitude rarefactive ion/electron acoustic solitary wave shows an increase in the width with increasing amplitude, and vice versa [*Ghosh and Lakhina*, 2004, 2005b]. However, those cases involved much larger normalized amplitude for the solutions. The extreme narrowness of the observed pulses, on the other hand, suggests its resemblance with the cusp-like solitary waves found in section 3.3. For a closer look, we have chosen a particular magnetosheath event of 11 April 2004. The analysis of the flight data from the Cluster PEACE [*Johnstone et al.*, 1997], CIS [*Rème et al.*, 2001], FGM [*Balogh et al.*, 2001], and Whisper Sounder [*Dècréau et al.*, 1997] instruments and the antenna modeling for the period 0046–0047 UT [*Béghin et al.*, 2005] showed that there were two electron components present with the following characteristics: n_{ec} = 16 cm^{-3}, n_{eh} = 8 cm^{-3}, T_{ec} = 39 eV, T_{eh} = 79 eV, the subscripts c (h) denoting the cooler (hotter) species, respectively, $\Omega_{ce}(B_0)$ = 1120 Hz (40 nT), $\omega_{pe}(n_0)$ = 44091 Hz (24 cm^{-3}), and $\tilde{u}_{eb} = 2.7896 \times 10^2$ km/s. The proton (H^+) temperature was found to be 200 eV while no information for He^{+2} was available.

[22] Taking these ion and electron data as input to our model, we have calculated α_e = 0.025 and ρ_{es} = 0.65 while $\sigma_{es}(\sigma_{eb})$ and u_{eb} have been calculated by normalizing T_{ec} (T_{eh}) and the electron beam velocity appropriately. Assuming $T_{He^{+2}} > T_{H^+}$, we have obtained positive polarity solutions with pulse durations of $\sim$1 ms and amplitudes $\geq$1 mV/m. The analytical estimation remains inconsistent with the observation. Knowing that a compressive solitary wave typically has smaller amplitude, we focused our attention on both compressive and rarefactive waves in this section. Also, considering the ion heating in the downstream region, we extend our analysis to include the $T_{He^{+2}} < T_{H^+}$ case as well. The results of our study have been summarized in the following sections.

4.2.1. Compressive Solitary Wave

[23] We have assumed a hotter species of He^{+2} ions with β_i = 0.54 and μ_i = 0.88. For M = 0.9 and θ = 30°, a compressive (negative polarity) electron acoustic solitary wave has been obtained. Figures 13a and 13b show the Sagdeev pseudopotential and potential profile, respectively. We have measured a normalized amplitude $\phi_0 = -0.0044$ and width w = 50.05 leading to the estimated values of E = 0.8181 mV/m and Δt = 0.2003 ms. These values remain quite close to the CLUSTER observations in the magnetosheath which detect an electric field fluctuation of $E \approx 0.04$–0.8 mV/m and pulse duration of $\Delta t \sim 0.05$–1.3 ms (Figure 15 and Table 3).

4.2.2. Rarefactive Solitary Wave

[24] For a rarefactive (positive polarity) solitary wave, a hotter species of He^{+2} ions yields a much larger amplitude compared to the observed one. On the other hand, a cooler species restricts the existence domain to a substantially narrow parameter regime. Figures 14a and 14b show the Sagdeev pseudopotential and the potential profile for the rarefactive solitary wave for $T_{He^{+2}} < T_{H^+}$ with β_i = 0.6

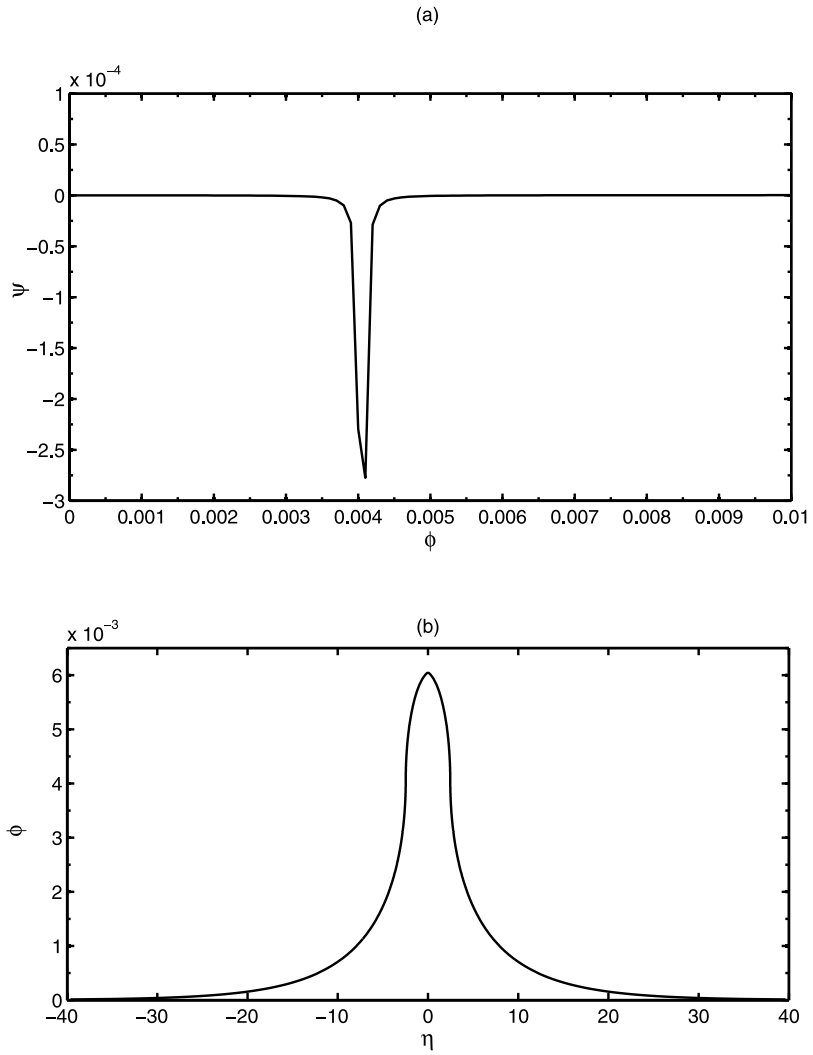

Figure 17. (a) The Sagdeev pseudopotential and (b) the potential profile of the electron acoustic solitary wave in the cusp. The plasma parameters are $\alpha_e = 0.015$, $\beta_i = 0.1$, $\rho_{es} = 0.6$, $\mu_i = 0.9$, $\sigma_{es} = 0.041$, $\sigma_{eb} = 0.0635$, $M = 0.9$, $\theta = 60°$, and $u_{eb} = 0.0628$.

and $\mu_i = 0.1$. The wave parameters are assumed to be $M = 0.7$ and $\theta = 60°$. The low value of $\mu_i = 0.1$ triggers a very small-amplitude ($\phi_0 = 0.0015$) and narrow profile ($w = 46.98$) with estimated values of $E = 0.2402$ mV/m and $\Delta t = 0.2418$ ms. The results are found to be in good agreement with the observation (Figure 15 and Table 3).

[25] For the completeness of our discussion, we have shown in Figure 15 the characteristics of solitary waves at the magnetosheath crossing as observed by the CLUSTER multispacecraft mission. Data shown in the figure correspond to the ESW characteristics obtained from the 11 April 2004 observations of the WBD receiver made in the magnetosheath at 11.5 R_E, 17.7 λ_M (geomagnetic latitude), and 0939 MLT (magnetic local time). The very narrow pulses of time duration of a tenth of a millisecond with amplitudes consistently below 1 mV/m are worth to be noted. As shown in Figure 3 of *Pickett et al.* [2008], most of the ESWs detected during this interval of time occurred when the angle of the detecting electric antenna was at a total angle of 45–75 degrees of the measured magnetic field direction, indicating a possible oblique propagation of these ESWs (see *Pickett et al.* [2008] for further explanation on this point). Our analytical estimations suggest that both negative and positive polarity solutions are possible in this region. The type and characteristics of the solitary wave depends crucially on the He^{+2} ion temperature. A hotter

Table 1. Comparison of ESWs for Different Regions of Space[a]

Bow Shock	Magnetosheath	Cusp
$T_{es} = 35$ eV	$T_{es} = 39$ eV	$T_e = 33.2$ eV
$T_{eb} = 28$ eV	$T_{eb} = 79$ eV	. . .
$T_{H+} = 300$ eV	$T_{H+} = 200$ eV	$T_{H+} = 600$ eV
. . .	. . .	$T_{O+} = 6000$ eV
$n_0 = 40$ cm^{-3}	$n_0 = 24$ cm^{-3}	$n_0 = 9.45$ cm^{-3}
. . .	$n_{ec} = 16$ cm^{-3}	. . .
. . .	$n_{eh} = 8$ cm^{-3}	. . .
$B_0 = 102$ nT	$B_0 = 40$ nT	$B_0 = 15$ nT
$\tilde{u}_{eb} =$ 650 km/s	$\tilde{u}_{eb} =$ 2.79×10^2 km/s	$\tilde{u}_{eb} =$ 6.76×10^2 km/s
$\omega_{pe} = 56921$ Hz	$\omega_{pe} = 44091$ Hz	$\omega_{pe} = 27667$ Hz
$\Omega_{ce} = 2856$ Hz	$\Omega_{ce} = 1120$ Hz	$\Omega_{ce} = 420$ Hz
$\alpha_e = 0.05$	$\alpha_e = 0.025$	$\alpha_e = 0.015$

[a] Plasma parameters obtained/estimated from the satellite observations.

Table 2. Comparison of ESWs for Different Regions of Space[a]

	Magnetosheath		
Bow Shock	Compressive	Rarefactive	Cusp
$\sigma_{es} = 0.1079$	$\sigma_{es} = 0.1969$	$\sigma_{es} = 0.2860$	$\sigma_{es} = 0.041$
$\sigma_{eb} = 0.0863$	$\sigma_{eb} = 0.3988$	$\sigma_{eb} = 0.5793$	$\sigma_{eb} = 0.0635$
$\rho_{es} = 0.98$	$\rho_{es} = 0.65$	$\rho_{es} = 0.65$	$\rho_{es} = 0.6$
$\mu_i = 0.85$	$\mu_i = 0.88$	$\mu_i = 0.1$	$\mu_i = 0.9$
$\beta_i = 0.25$	$\beta_i = 0.54$	$\beta_i = 0.6$	$\beta_i = 0.1$
($T_{He^{2+}} = 1200$ eV)	($T_{He^{2+}} = 370.37$ eV)	($T_{He^{2+}} = 120$ eV)	(see Table 1)
$u_{eb} = 0.0861$	$u_{eb} = 0.0473$	$u_{eb} = 0.0570$	$u_{eb} = 0.0628$
$M = 0.77$	$M = 0.9$	$M = 0.7$	$M = 0.9$
$\theta = 75°$	$\theta = 30°$	$\theta = 60°$	$\theta = 60°$

[a] Inputs estimated/assumed for the model.

species of He^{+2} ion favors a compressive solution while a cooler species will support a positive polarity solution. It also suggests that the existence of the acoustic mode is restricted to a narrow parameter regime and the abundance of observed solitary structures may result from a narrow band of He^{+2} ions, though the presence of other competitive processes can not be ruled out. The measurement of the He^{+2} ion temperature thus becomes necessary to validate the generation mechanism of ESWs in the magnetosheath. Nevertheless, the acoustic mode solution remains a strong candidate for the region. A more detailed investigation of the magnetosheath is, though necessary, out of the scope of the present work and will be communicated elsewhere.

4.3. Cusp

[26] Figure 16 shows the characteristics of electrostatic solitary waves at a cusp crossing. For this event most of the ESWs were detected at angles of the electric antenna to the magnetic field of 35–65 degrees (not shown), once again suggesting oblique propagation. For the sake of comparison, we have chosen the particular cusp event of 19 February 2002, 2324:11 UT while the spacecraft was located at $\sim$11 R_E, 60 λ_M, and 14 h MLT. The data correspond to the 19 February 2002 observations made by the WBD receiver on board the CLUSTER 1 spacecraft. The data analysis shows two components of ion populations, namely, H^+(=600 eV) and O^+(=6000 eV) while the measured electron temperature was $\sim$33.2 eV. Other plasma parameters detected from the data analysis are as follows: $\Omega_{ce}(B_0)$ = 420 Hz (15 nT), $\omega_{pe}(n_0)$ = 27667 Hz (9.45 cm^{-3}), and $\tilde{u}_{eb}$ = 6.7658 $\times$ 10^2 km/s. This leads to $\alpha_e = 0.015$, $\beta_i = 0.1$ and an average electron to ion temperature ratio $\sigma_e \approx 0.05$. In the absence of any data for two electron populations, we have assumed $\rho_{es} = 0.6$, σ_{es} (σ_{eb}) = 0.041 (0.064) while the wave parameters are assumed to be $M = 0.9$ and $\theta = 60°$. We have also assumed a 10% population for oxygen ions ($\mu_i = 0.9$). The corresponding solitary wave solution has been shown in Figures 17a and 17b. The amplitude ($\phi_0 = 0.0061$) and the width ($w = 21.8333$) of the analytical solution lead to the estimated values of $E = 2.9792$ mV/m and $\Delta t = 0.1328$ ms.

[27] A comparison between Figures 16 and 17 shows good agreement between the pulse durations. However, the theoretical value of the electric field E remains grossly overestimated. The comparatively large-amplitude solution results due to the presence of high-energy ions. The sources of such discrepancies may lie in discarding wave-particle interactions like Landau damping or particle trapping which are beyond the scope of the present analytical model. It has been observed that an increase in the plasma density reduces the amplitude considerably. Inclusion of kinetic processes in the model may thus become necessary to reproduce the observational results more accurately in this region. The findings of the comparison between the analytical model and space observations are summarized in Tables 1–3.

5. Conclusion

[28] We have studied the parametric dependence of the electron acoustic solitary wave in detail. We have also studied the effect of ion parameters on the electron acoustic WDL. The importance of the presence of the second ion species becomes evident in our analysis. It leads us to the discovery of narrow cusp-like solitary waves (section 3.3). We have noted that such cusp-like solutions occur specifically for an oblique propagation of the wave in a magnetized plasma and not expected for a parallel propagation. Given the fact that at different regions of the magnetosphere

Table 3. Comparison of ESWs for Different Regions of Space[a]

		Solitary Wave		
		Theory		
Region	Normalization Parameters	Normalized	Nonnormalized	Observations
Bow shock	$T_{iff} = 324.3243$ eV	$\phi_0 = 0.4866$	$E = 141.06$ mV/m	$E \approx 150$ mV/m
	$\lambda_{Diff} = 21.0713$ m	$w = 53.0899$	$\Delta t = 0.1924$ ms	$\Delta t \sim 0.1$ ms
	$c_{iff} = 7.5514 \times 10^3$ km/s			
Magnetosheath		*Compressive Wave*		
	$T_{iff} = 198.0983$ eV	$\phi_0 = -0.0044$	$E = 0.8181$ mV/m	$E \approx 0.04$–0.8 mV/m
	$\lambda_{Diff} = 21.2602$ m	$w = 50.0546$	$\Delta t = 0.2003$ ms	$\Delta t \sim 0.05$–1.3 ms
	$c_{iff} = 5.9017 \times 10^3$ km/s			
		Rarefactive Wave		
	$T_{iff} = 136.3636$ eV	$\phi_0 = 0.0015$	$E = 0.2402$ mV/m	
	$\lambda_{Diff} = 17.6391$ m	$w = 46.9813$	$\Delta t = 0.2418$ ms	
	$c_{iff} = 4.8965 \times 10^3$ km/s			
Cusp	$T_{iff} = 659.3407$ eV	$\phi_0 = 0.0061$	$E = 2.9792$ mV/m	$E \approx 0.01$–1 mV/m
	$\lambda_{Diff} = 61.3269$ m	$w = 21.8333$	$\Delta t = 0.1328$ ms	$\Delta t \sim 0.1$–1 ms
	$c_{iff} = 1.0767 \times 10^4$ km/s			

[a] Solitary wave solutions.

the hotter species of ions comprises the minority component, these cusp-like solitary waves have emerged as a more suitable candidate for modeling the observed ESWs in those regions. Though it is difficult to reproduce the observations from an analytical model, the agreements are quite encouraging. We have shown that, in the magnetosheath, both positive and negative polarity solutions are possible depending upon the He^{+2} ion temperature with respect to protons. We have also shown that an electron acoustic solitary wave satisfactorily models the observed ESWs in the magnetosheath. In the bow shock, the model estimates large-amplitude ESWs which results due to the compression of the magnetic field but predicts a comparatively lower amplitude at the upstream. According to our model, the electron beam is assumed to be highly collimated having only the z component of motion along the ambient magnetic field. As we expect a much slower timescale of the turbulence at the bow shock or the magnetosheath compared to the high-frequency part of the ESW, our model remains applicable at those regions. A more realistic model is, though necessary, out of the scope of the analytical investigation and can be solved only numerically. It is interesting to note that the CLUSTER observations detected the greatest occurrence of ESWs at rather oblique angles of the electric antenna to the measured magnetic field as opposed to the antenna being nearly aligned with the magnetic field as expected for propagation along the magnetic field. Such observations are consistent with our model which assumes an oblique propagation. However, there could be other explanations for these observed angles other than an oblique propagation and it needs to be investigated in more detail. There are some discrepancies observed in the estimation of the amplitude in the cusp region. There is always the possibility of the coexistence of different generation mechanisms and a more detailed analysis of the region is expected to complement our present findings.

[29] **Acknowledgments.** The authors acknowledge the FGM instrument investigation team and the Cluster Active Archive for the Cluster magnetic field data. Part of the work has been completed under JSPS fellowship of Japan at Computer Science Laboratory, RISH, Kyoto University, Japan. One of the author, S. S. Ghosh, thanks Y. Omura and other group members of RISH for their constant help and support. The authors also thank B. T. Tsurutani of JPL, NASA and R. Pottelette of CETP/CNRS, France for helpful discussions. G. S. Lakhina would like to thank the Council of Scientific and Industrial Research (CSIR), Government of India, for the support under the Emeritus Scientist Scheme. J. S. Pickett acknowledges support from NASA GSFC under grants NNG04GB09G and NNX07AI24G.

[30] Amitava Bhattacharjee thanks X.H. Deng and another reviewer for their assistance in evaluating this paper.

References

Bale, S., P. Kellogg, D. Larson, R. Lin, K. Goetz, and R. Lepping (1998), Bipolar electrostatic structures in the shock transition region: Evidence of electron phase space holes, *Geophys. Res. Lett.*, *25*, 2929–2932.

Balogh, A., et al. (2001), The CLUSTER magnetic field investigation: Overview of in-flight performance and initial results, *Ann. Geophys.*, *19*, 1207–1217.

Baumjohann, W., G. Paschmann, and A. Cattell (1989), Average plasma properties in the central plasma sheet, *J. Geophys. Res.*, *94*, 6597–6606.

Béghin, C., P. M. E. Décréau, J. Pickett, D. Sundkvist, and B. Lefebvre (2005), Modeling of CLUSTER's electric antennas in space: Application to plasma diagnostics, *Radio Sci.*, *40*, RS6008, doi:10.1029/2005RS003264.

Berthomier, M., R. Pottelette, M. Malingre, and Y. Khotyaintsev (2000), Electron acoustic solitons in an electron–beam plasma system, *Phys. Plasmas*, *7*, 2987–2994.

Bharuthram, R., and P. K. Shukla (1988), Nonlinear properties of electron acoustic wave turbulence in the geomagnetic tail, *Astrophys. Space Sci.*, *149*, 127–140.

Böstrom, R., G. Gustafsson, B. Holback, G. Holmgren, H. Koshkinen, and P. Kintner (1988), Characteristics of solitary waves and double layers in the magnetospheric plasma, *Phys. Rev. Lett.*, *61*, 82–85.

Bounds, S. R., R. F. Pfaff, S. F. Knowlton, F. S. Mozer, M. A. Temerin, and C. A. Kletzing (1999), Solitary potential structures associated with ion and electron beams near 1 R_E altitudes, *J. Geophys. Res.*, *104*, 28,709–28,717.

Buti, B. (1980), Nonlinear electron-acoustic wave in a multi-species plasma, *J. Plasma Phys.*, *24*, 169–180.

Buti, B., M. Mohan, and P. K. Shukla (1980), Exact electron acoustic solitary waves, *J. Plasma Phys.*, *23*, 341–347.

Cattell, C. A., et al. (1999), Comparisons of POLAR satellite observations of solitary wave velocities in the plasma sheet boundary and the high altitude cusp to those in the auroral zone, *Geophys. Res. Lett.*, *26*, 425–428.

Cattell, C. A., J. Crumley, J. Dombeck, R. Lysak, C. Kletzing, W. K. Peterson, and C. Collin (2001), POLAR observations of solitary waves at high and low altitudes and comparison to theory, *Adv. Space Res.*, *28*, 1631–1641.

Cattell, C. A., et al. (2005), CLUSTER observations of electron holes in association with magnetotail reconnection and comparison to simulations, *J. Geophys. Res.*, *110*, A01211, doi:10.1029/2004JA010519.

Dècréau, P. M. E., et al. (1997), Whisper, a resonance sounder and wave analyzer: Performances and perspectives for the CLUSTER mission, *Space Sci. Rev.*, *79*, 157–193.

Deng, X. H., et al. (2004), GEOTAIL encounter with reconnection diffusion region in the earth's magnetotail: Evidence of multiple x lines collisionless reconnection?, *J. Geophys. Res.*, *109*, A05206, doi:10.1029/2003JA010031.

Dubouloz, N., R. Pottelette, M. Malingre, G. Holmgren, and P. A. Lindqvist (1991a), Detailed analysis of broadband electrostatic noise in the dayside auroral zone, *J. Geophys. Res.*, *96*, 3565–3579.

Dubouloz, N., R. Pottelette, M. Malingre, and R. A. Treumann (1991b), Generation of broadband electrostatic noise by electron acoustic solitons, *Geophys. Res. Lett.*, *18*, 155–158.

Dubouloz, N., R. A. Treumann, R. Pottelette, and M. Malingre (1993), Turbulence generated by a gas of electron acoustic solitons, *J. Geophys. Res.*, *98*, 17,415–17,422.

Dupree, T. H. (1982), Theory of phase space density holes, *Phys. Fluids*, *25*, 277–289.

El-Taibany, W. F. (2005), Electron acoustic solitary waves and double layers with an electron beam and phase space electron vortices in space plasmas, *J. Geophys. Res.*, *110*, A01213, doi:10.1029/2004JA010525.

Ergun, R. E., et al. (1998a), FAST satellite observations of large amplitude solitary structures, *Geophys. Res. Lett.*, *25*, 2041–2044.

Ergun, R. E., C. W. Carlson, J. P. McFadden, F. S. Mozer, L. Muschietti, I. Roth, and R. Strangeway (1998b), Decay–scale plasma structures associated with magnetic–field–aligned electric fields, *Phys. Rev. Lett.*, *81*, 826–829.

Franz, J., P. Kintner, and J. Pickett (1998), POLAR observations of coherent electric field structures, *Geophys. Res. Lett.*, *25*, 1277–1280.

Fried, D. B., and R. W. Gould (1961), Longitudinal ion oscillations in a hot plasma, *Phys. Fluids*, *4*, 139–147.

Gary, S. P., and R. L. Tokar (1985), The electron acoustic mode, *Phys. Fluids*, *28*, 2439–2441.

Ghosh, S. S., and A. N. S. Iyengar (1997), Anomalous width variations for ion acoustic rarefactive solitary waves in a warm ion plasma with two electron temperatures, *Phys. Plasmas*, *5*, 3204–3210.

Ghosh, S. S., and G. S. Lakhina (2004), Anomalous width variation of rarefactive ion acoustic solitary waves in the context of auroral plasmas, *Nonlin. Process. Geophys.*, *11*, 219–228.

Ghosh, S. S., and G. S. Lakhina (2005a), Beam driven electron acoustic solitary waves in multi-ion plasma, paper presented at 2005 Scientific Assembly, Int. Assoc. of Geomagn. and Aeron., Toulouse, France, 18–29 July.

Ghosh, S. S., and G. S. Lakhina (2005b), Width–amplitude variation of positive amplitude electron acoustic solitary wave, paper presented at XXVIIIth General Assembly, Int. Union of Radio Sci., New Delhi, 23–29 October.

Goldman, M. V., M. M. Oppenheim, and D. L. Newman (1999), Nonlinear two–stream instabilities as an explanation for auroral bipolar wave structures, *Geophys. Res. Lett.*, *26*, 1821–1824.

Gurnett, D. A., R. L. Huff, and D. L. Kirchner (1997), The wide-band plasma wave investigation, *Space Sci. Rev.*, *79*, 195–208.

Johnstone, A. D., et al. (1997), PEACE: A plasma electron and current experiment, *Space Sci. Rev.*, *79*, 351–398.

Kalra, G. L., and S. Kumar (2006), Effect of He^{++} ions on the propagation of low–frequency magnetohydrodynamic waves in the magnetosheath, *J. Geophys. Res.*, *111*, A11226, doi:10.1029/2005JA011453.

Lashmore-Davies, C. N., and T. J. Martin (1973), Electrostatic instabilities driven by an electric current perpendicular to a magnetic field, *Nucl. Fusion*, *13*, 193–203.

Lin, C. S., D. Winske, and R. L. Tokar (1985), Simulation of electron acoustic instability in the polar cusp, *J. Geophys. Res.*, *90*, 8269–8280.

Mace, R. L., and M. A. Hellberg (1990), Higher order electron modes in a two electron temperature plasma, *J. Plasma Phys.*, *43*, 239–255.

Mace, R. L., and M. A. Hellberg (1993), Electron-acoustic and cyclotron-sound instabilities driven by field-aligned hot-electron streaming, *J. Geophys. Res.*, *98*, 5881–5891.

Mace, R. L., S. Baboolal, R. Bharuthram, and M. A. Hellberg (1991), Arbitrary amplitude electron acoustic solitons in a two-electron-component plasma, *J. Plasma Phys.*, *45*, 323–338.

Mamun, A. A., and P. K. Shukla (2002a), Obliquely propagating electron–acoustic solitary waves, *Phys. Plasmas*, *9*, 1474–1477.

Mamun, A. A., and P. K. Shukla (2002b), Electron-acoustic solitary waves via vortex electron distribution, *J. Geophys. Res.*, *107*(A7), 1135, doi:10.1029/2001JA009131.

Mangeney, A., et al. (1999), WIND observations of coherent electrostatic waves in the solar wind, *Ann. Geophys.*, *17*, 307–320.

Matsumoto, H. H., H. Kojima, T. Miyatake, Y. Omura, M. Okada, I. Nagano, and M. Tsutsui (1994a), Electrostatic solitary waves (ESW) in the magnetotail: BEN waveforms observed by GEOTAIL, *Geophys. Res. Lett.*, *21*, 2915–2918.

Matsumoto, H. H., et al. (1994b), Plasma wave observations with GEOTAIL spacecraft, *J. Geomag. Geoelectr.*, *46*, 59–95.

Matsumoto, H. H., H. Kojima, Y. Kasaba, T. Miyake, R. R. Anderson, and T. Mukai (1997), Plasma waves in the upstream and bow shock regions observed by GEOTAIL, *Adv. Space. Res.*, *20*, 683–693.

McFadden, J. P., C. W. Carlson, and R. E. Ergun (1999), Microstructure of the auroral acceleration region as observed by FAST, *J. Geophys. Res.*, *104*, 14,453–14,480.

Mozer, F. S., R. Ergun, M. Temerin, C. Cattell, J. Dombeck, and J. Wygant (1997), New features of time domain electric field structures in the auroral acceleration region, *Phys. Rev. Lett.*, *79*, 1281–1284.

Muschietti, L., R. E. Ergun, I. Roth, and C. W. Carlson (1999), Phase space electron holes along magnetic field lines, *Geophys. Res. Lett.*, *26*, 1093–1096.

Newman, D. L., M. V. Goldman, R. E. Ergun, and A. Mangeney (2001), Formation of double layers and electron holes in a current driven space plasma, *Phys. Rev. Lett.*, *87*, 1–4.

Omura, Y., H. Kojima, and H. Matsumoto (1994), Computer simulation of electrostatic solitary waves: A nonlinear model of broadband electrostatic noise, *Geophys. Res. Lett.*, *21*, 2923–2926.

Parks, G. K., et al. (1984), Particle and field characteristics of the high lattitude plasma sheet boundary layer, *J. Geophys. Res.*, *89*, 8885–8906.

Pickett, J. S., et al. (1999), Plasma waves observed during cusp energetic particle events and their correlation with POLAR and AKEBONO satellite and ground data, *Adv. Space Res.*, *24*, 23–33.

Pickett, J. S., J. D. Menietti, D. A. Gurnett, B. T. Tsurutani, P. M. Kintner, E. Klatt, and A. Balogh (2003), Solitary potential structures observed in the magnetosheath by the CLUSTER spacecraft, *Nonlinear Proc. Geophys.*, *10*, 3–11.

Pickett, J. S., L. J. Chen, S. W. Kahler, O. Santolik, D. A. Gurnett, B. T. Tsurutani, and A. Balogh (2004), Isolated electrostatic structures observed throughout the CLUSTER orbit: Relationship to magnetic field strength, *Ann. Geophys.*, *22*, 2515–2523.

Pickett, J. S., et al. (2008), Furthering our understanding of electrostatic solitary waves through CLUSTER multispacecraft observations and theory, *Adv. Space Res.*, *41*, 1666–1676, doi:10.1016/jasr.2007.05.064.

Pottelette, R., R. E. Ergun, R. A. Treumann, M. Berthomier, C. W. Carlson, J. P. McFadden, and I. Roth (1999), Modulated electron acoustic waves in auroral density cavities: FAST obsevations, *Geophys. Res. Lett.*, *26*, 2629–2632.

Rème, H., et al. (2001), First multispacecraft ion measurements in and near the earth's magnetosphere with the identical CLUSTER ion spectrometry (CIS) experiment, *Ann. Geophys.*, *19*, 1303–1354.

Schriver, D., and M. A. Ashour-Abdalla (1987), Generation of high frequency broadband electrostatic noise: The role of cold electrons, *J. Geophys. Res.*, *92*, 5807–5819.

Shin, K., H. Kojima, H. Matsumoto, and T. Mukai (2006), Electrostatic quasi-monochromatic waves in the downstream region of the earth's bow shock based on GEOTAIL observations, *Earth Planets Space*, *58*, 1–7.

Singh, N. (2000), Electron holes as a common feature of double-layer-driven plasma waves, *Geophys. Res. Lett.*, *27*, 927–930.

Singh, S. V., and G. S. Lakhina (2001), Generation of the electron acoustic waves in the magnetosphere, *Planet. Space Sci.*, *49*, 107–114.

Singh, S. V., and G. S. Lakhina (2004), Electron acoustic solitary waves with non-thermal distribution of electrons, *Nonlinear Proc. Geophys.*, *11*, 275–279.

Singh, S. V., R. V. Reddy, and G. S. Lakhina (2001), Broadband electrostatic noise due to nonlinear electron acoustic wave, *Adv. Space Res.*, *28*, 1643–1648.

Sutradhar, S., and S. Bujarbarua (1988), Electron acoustic double layer in a current carrying magnetized plasma, *Planet Space Sci.*, *36*, 1009–1013.

Temerin, M., K. Cerny, W. Lotko, and F. S. Mozer (1982), Observations of solitary waves and double layers in the auroral plasma, *Phys. Rev. Lett.*, *48*, 1175–1179.

Tokar, R. L., and S. P. Gary (1984), Electrostatic hiss and the beam driven electron acoustic instability in the dayside polar cusp, *Geophys. Res. Lett.*, *11*, 1180–1183.

Tsurutani, B. T., C. M. Ho, G. S. Lakhina, B. Buti, J. K. Arballo, J. S. Pickett, and D. A. Gurnett (1998), Plasma waves in the dayside polar cap boundary layer: Bipolar and monopolar electric pulses and whistler mode waves, *Geophys. Res. Lett.*, *25*, 4117–4120.

Watanabe, K., and T. Taniuti (1977), Electron acoustic mode in a plasma of two-temperature electrons, *J. Phys. Soc. Jpn.*, *43*, 1819–1820.

Wei, R., and Y. Chen (2005), Nonlinear lower hybrid waves in two-ion-species plasmas, *Phys. Scr.*, *71*, 648–651.

Williams, J. D., L. J. Chen, W. S. Kurth, D. A. Gurnett, M. K. Dougherty, and A. M. Rymer (2005), Electrostatic solitary structures associated with the November 10, 2003 interplanetary shock at 8.7 AU, *Geophys. Res. Lett.*, *32*, L17103, doi:10.1029/2005GL023079.

Williams, J. D., L. J. Chen, W. S. Kurth, D. A. Gurnett, and M. K. Dougherty (2006), Electrostatic solitary structures observed at Saturn, *Geophys. Res. Lett.*, *33*, L06103, doi:10.1029/2005GL024532.

Yu, M. Y., and P. K. Shukla (1983), Linear and nonlinear modified electron acoustic waves, *J. Plasma Phys.*, *29*, 409–413.

P. M. E. Décréau, LPCE et Université d'Orléans, 3A, Avenue de la Recherche Scientifique, F-45071 Orléans CEDEX 2, France.

S. S. Ghosh and G. S. Lakhina, Indian Institute of Geomagnetism, Plot 5, Sector 18, New Panvel (W), Navi Mumbai, 410218, India. (sukti@iigp.iigm.res.in)

B. Lavraud, Los Alamos National Laboratory, Los Alamos, NM 87545, USA.

J. S. Pickett, University of Iowa, Iowa City, IA 52242, USA.

J. D. Winningham, Southwest Research Institute, P. O. Drawer 28510, 6220 Culebra Road, San Antonio, TX 78228-0510, USA.